

microRNA-324 mediates bone homeostasis and the regulation of osteoblast and osteoclast differentiation and activity



Dan J. Hayman, Francesca M. Johnson de Sousa Brito, Hua Lin, Amanda Prior, Gemma Charlesworth, Yao Hao, Rachel D. Pearson, Jamie Soul, Ian M. Clark, Katarzyna A. Piróg, Matt J. Barter, Rob J. Van't Hof, David A. Young

PII: S8756-3282(24)00262-X

DOI: <https://doi.org/10.1016/j.bone.2024.117273>

Reference: BON 117273

To appear in: *Bone*

Received date: 13 July 2024

Revised date: 24 September 2024

Accepted date: 3 October 2024

Please cite this article as: D.J. Hayman, F.M. Johnson de Sousa Brito, H. Lin, et al., microRNA-324 mediates bone homeostasis and the regulation of osteoblast and osteoclast differentiation and activity, *Bone* (2024), <https://doi.org/10.1016/j.bone.2024.117273>

This is a PDF file of an article that has undergone enhancements after acceptance, such as the addition of a cover page and metadata, and formatting for readability, but it is not yet the definitive version of record. This version will undergo additional copyediting, typesetting and review before it is published in its final form, but we are providing this version to give early visibility of the article. Please note that, during the production process, errors may be discovered which could affect the content, and all legal disclaimers that apply to the journal pertain.

Title

microRNA-324 mediates bone homeostasis and the regulation of osteoblast and osteoclast differentiation and activity

Authors

Dan J. Hayman^a, Francesca M. Johnson de Sousa Brito^a, Hua Lin^a, Amanda Prior^b, Gemma Charlesworth^b, Yao Hao^{a,1}, Rachel D. Pearson^a, Jamie Soul^{a,2}, Ian M. Clark^c, Katarzyna A. Piróg^a, Matt J. Barter^a, Rob J. van 't Hof^b, David A. Young^{a*}

^aBiosciences Institute, Newcastle University, Central Parkway, Newcastle upon Tyne, NE1 3BZ, UK

^bDepartment of Musculoskeletal Biology, Institute of Ageing and Chronic Disease, University of Liverpool, Liverpool, L69 7TX, UK

^cSchool of Biological Sciences, University of East Anglia, Norwich, NR4 7TJ, UK

***Corresponding author.** Tel: +44 191 2418831; FAX: Not applicable; Email: d.a.young@ncl.ac.uk

Footnotes

¹Orthopedics Department, First Hospital of Shanxi Medical University, Taiyuan, China

²Computational Biology Facility, Faculty of Health and Life Sciences, University of Liverpool, Liverpool, L69 7TX, UK

Concise running title: miR-324 controls bone homeostasis

Author Contributions

DAY, IMC, MJB, DJH and RVH conceived and designed the work that led to the submission. DJH, HL, AP, GC, YH, RDP and MJB acquired data. DJH, FJSB, RDP, JS, KAP, MJP, RVH and DAY interpreted the results. DJH, DAY, FJSB, RDP and RVH drafted or revised the manuscript. All authors approved the final manuscript.

Author email addresses

Dan J. Hayman < d.j.hayman@sheffield.ac.uk >

Francesca M. Johnson de Sousa Brito < francesca.de-sousa-brito@newcastle.ac.uk >

Hua Lin < hua.lin7181@gmail.com >

Amanda Prior < aprior@liverpool.ac.uk >

Gemma Charlesworth <gemma@liverpool.ac.uk>

Yao Hao <haoyao1985@hotmail.com>

Rachel D. Pearson <r.d.pearson@newcastle.ac.uk>

Jamie Soul <jamie.soul@liverpool.ac.uk>

Ian M. Clark <i.clark@uea.ac.uk>

Katarzyna A. Piróg <katarzyna.pirog@newcastle.ac.uk>

Matt J. Barter <matthew.barter@newcastle.ac.uk>

Rob Van 'T Hof <rj.vanthof@gmail.com>

David A. Young <d.a.young@ncl.ac.uk>

Conflict of interest: None

Abstract

MicroRNAs (miRNAs) modulate the expression of other RNA molecules. One miRNA can target many transcripts, allowing each miRNA to play key roles in many biological pathways. Defects in bone homeostasis result in the common age-related diseases including osteoporosis. Serum level of miR-324-3p positively correlate with several features of bone maintenance. In contrast here, using *in vivo* micro-computed tomography and histology, global miR-324-null mice demonstrated increased bone mineral density and both trabecular and cortical thickness, with effect magnitudes increasing with age. The bone marrow of miR-324-null mice had reduced lipid content while TRAP staining revealed a decrease in osteoclasts, with histomorphometry demonstrating an increased rate of bone formation. *Ex vivo* assays showed that the high bone mass phenotype of miR-324-null mice resulted from both increased osteoblast activity and decreased osteoclastogenesis. RNA-seq analysis of osteoblasts, osteoclasts and bone marrow macrophages and target validation assays identified that the osteoclast fusion regulator *Pin1* and the master osteogenic regulator *Runx2* were targets of miR-324-5p in osteoclast lineage cells and osteoblasts, respectively. Indeed, *in vitro* *Runx2* overexpression recapitulated the increased osteogenesis and decreased adipogenesis phenotype observed *in vivo* by the loss of miR-324. Overall, these data demonstrate the importance of miR-324 in bone homeostasis by regulating aspects of both bone formation and remodelling. Elucidation of pathways regulated by miR-324 offer promise for the treatment of bone diseases such as osteoporosis.

Keywords

microRNA, osteoclast, osteoblast, bone

1. Introduction

MicroRNAs (miRNAs) are a class of ncRNA which modulate the expression of target RNA molecules through complimentary binding to, usually, the 3' untranslated region (3'UTR) of target mRNAs. Consequently, the mRNA target is generally degraded. One miRNA can target many mRNAs and each mRNA is often the target of multiple miRNAs [1].

With an ageing demographic, musculoskeletal conditions are increasing in prevalence. The most common musculoskeletal conditions are osteoarthritis (OA) and osteoporosis (OP) [2, 3]. Treatments for OA are limited to analgesic use prior to eventual joint replacement. For OP therapeutic options are better and range from supplements (e.g., calcium and vitamin D), through to hormone replacement, bisphosphonates and more recently biologics such as Denosumab and Romosozumab, amongst other treatments [3].

Bone remodelling is a crucial process, responsible for the maintenance of bone mass [4]. It is comprised of antagonistic effects provided by osteoblasts and osteoclasts, along with osteocytes, which regulate the balance and activity of the former [5]. The differentiation of these cells from mesenchymal and haematopoietic stem cells in the bone marrow is cross-regulated by mature bone cells, such that bone remodelling can be precisely modulated according to the need of the skeletal system at a particular time. miRNAs play numerous roles in the processes involved in bone remodelling. To date, more than 80 miRNAs have been reported to affect either osteogenesis, osteoclastogenesis or the mediation of these processes by osteocytes [6]. For example, the miR-185-null mouse exhibits dramatically increased bone formation due to increased osteogenesis [7], whereas miR-124 targets NFATc1, the transcription factor responsible for activation of osteoclastogenic genes, thus acting to repress osteoclastogenesis [8]. Due to the complex networks through which these processes communicate, a single miRNA can therefore have large implications on the underlying balance between bone formation and resorption.

miR-324 has been associated with bone disease, including increased bone formation and as a serum marker for fracture risk [9-12]. miR-324 can reportedly regulate aspects of the Hedgehog (Hh) signalling [12-14], a pathway instrumental for many musculoskeletal processes including endochondral ossification, whereby cartilage tissue is replaced by bone [15]. Here we demonstrate that in a global knockout mouse model of *Mir324*, animals display a high bone mass phenotype, resulting from both a decrease in osteoclastogenesis and an increase in bone formation. Finally, we functionally define bone development and disease-relevant targets of miR-324.

2. Methods

2.1. miR-324-null mice

miR-324-null mouse model were generated as previously described with deletion of both arms of miR-324 (i.e., -5p and -3p) confirmed by qRT-PCR ([16] and Supplementary Figure S1). Mice were maintained on an inbred C57BL6 background. All mouse experiments were performed in compliance with the ARRIVE guidelines (<https://www.nc3rs.org.uk/arrive-guidelines>) [16] under license (P8A8B649A) granted from the Home Office (United Kingdom) in accordance with the guidelines and regulations for the care and use of laboratory animals outlined by the Animals (Scientific Procedures) Act 1986 according to Directive 2010/63/EU of the European Parliament. Protocols were approved by the Animal Ethics Committee of Newcastle University and the Home Office, United Kingdom. Genotyping of the mice was by PCR (Supplemental Table S1a) of genomic DNA from ear-notches as previously described [16]. Mice were euthanised by cervical dislocation. For the micro-computed tomography (μ CT) mice analysed were aged 5, 7 or 14-months and all males. For the other individual experimental procedures age and gender distribution are provided, where relevant.

2.2. Extraction of nucleic acids from murine tissues and cells

Total RNA was extracted from murine osteoblasts, osteoclasts and BMMs using the mirVana miRNA Isolation Kit (ThermoFisher Scientific), following the manufacturer's protocols. RNA concentration and purity was measured using an Agilent Bioanalyzer 2100 if used for RNA-sequencing. For cells cultured in 96-well plates, the Cells-to-cDNA II Kit (ThermoFisher Scientific) was used for RNA isolation with cDNA synthesis as described [17]. Genomic DNA was extracted from murine C3H10T1/2 cells using the PureLink Genomic DNA Mini Kit (ThermoFisher Scientific).

2.3. Real-time reverse transcriptase quantitative PCR (RT-qPCR)

cDNA synthesis was performed using MMLV reverse transcriptase and random hexamers according to the manufacturer's protocol (ThermoFisher Scientific, Loughborough, UK). For miRNAs, cDNA was synthesised from total RNA using TaqMan® MicroRNA Reverse Transcription (ThermoFisher Scientific) according to the manufacturer's instructions. TaqMan RT-qPCR was performed, and gene expression levels calculated as previously described [12, 17]. Primers/Assay are listed in Supplementary Table S1b, as are the Universal Probe Library probes used (Roche) where applicable. MiRNA expression was normalised to *U6* while other genes of interest (GOI) were normalised to *18S*.

2.4. RNA sequencing

Prior to RNA sequencing (RNA-seq), RNA samples were treated using the DNA-free™ DNA Removal Kit (ThermoFisher Scientific) to remove any DNA contamination. Sequencing libraries were prepared using the NEBNext® Single Cell/Low Input RNA Library Prep Kit for Illumina® (New England Biolabs) following the manufacturer's protocol and sequenced with an Illumina NovaSeq 6000. Kallisto [18] was used for pseudo-alignment and quantification, against the mouse GRCh38 (release 92) transcriptome [19]. Mapped transcripts were converted to a gene level using Tximport [20] and DESeq2 [21] was used to calculate p-values and \log_2 fold-changes (\log_2 FC), using the Benjamini-Hochberg method to adjust for multiple testing. All RNA-seq data generated is freely available on NCBI GEO (accession GSE226615). EnrichR was utilised for some Gene Ontology analysis and to define cells present in miR-324-null and WT osteoclast and BMM samples, using the PanglaoDB Augmented 2021 database with the top 500 most highly expressed genes with human orthologues, determined by average normalised count [22, 23].

2.5. Prediction of novel miR-324 targets

Genes upregulated (adjusted p-value ≤ 0.05 and $\log_2\text{FC} > 0.35$) in miR-324-null osteoblast and BMM RNA-seq samples were filtered using TargetScan [1] to predict targets of miR-324-5p and -3p with a total context score of < -0.25 . These genes were filtered for those annotated to bone- and metabolism-related DO terms [24] (Supplementary Table S2). The 3'UTRs of genes that passed all filters and thresholds were subsequently tested for direct interaction with miR-324-5p or -3p using 3'UTR-luciferase assays. miRmap [25] identified an additional miR-324-3p binding site in *Cxcl12-γ* by allowing for a non-canonical G-U base pairing.

2.6. Construction of 3'UTR luciferase reporter plasmids

Fragments of the 3'UTR regions of predicted miR-324 targets were PCR amplified (using Phire Hot Start II DNA Polymerase; ThermoFisher Scientific) from murine genomic DNA or osteoblast cDNA and cloned by In-Fusion HD cloning (Takara Bio) into the pmiRGLO luciferase reporter plasmid (Promega) previously linearised by *Xba*I restriction digestion, essentially as previously described [26].

Oligonucleotides are presented in Supplementary Table S1c. Mutant 3'UTR constructs, where 2 nucleotides within the predicted miR-324 binding sites were mutated, were cloned from gBlocks (Integrated DNA Technologies; Supplementary Table S1d) or for *Ptgs1* generated by site-directed mutagenesis using the QuikChange Lightning Site-Directed Mutagenesis Kit (Agilent Technologies) (Supplemental Table S1a). All constructs underwent confirmation by Sanger sequencing.

2.7. 3'UTR-luciferase assays

Murine C3H10T1/2 cells were cultured in DMEM-complete (medium supplemented with 2 mM L-glutamine, 10% foetal bovine serum (FBS), 100 µg/ml streptomycin and 100 IU/ml penicillin) and plasmid transfected essentially as previously described [12]. Four hours post plasmid transfection, media was aspirated, and the cells were transfected with 50 nM miCon, miR-324-5p or miR-324-3p mimics (Horizon Discovery) using DharmaFECT 1 (Horizon Discovery) transfection reagent. After 24 hours, luciferase and Renilla levels were quantified using a GloMax-Multi Detection System (Promega) and the Dual-Luciferase Reporter Assay System (Promega) [12]. Each condition consisted of ≥ 3 technical replicates and the mean from ≥ 3 independent experiments were used to calculate statistical significance using Student's two-tailed paired *t*-tests.

2.8. Protein extraction and immunoblotting

Murine tissue and cells samples were processed using a 1% (v/v) TritonX lysis buffer, as previously described [16]. Lysates were resolved by sodium dodecyl sulphate polyacrylamide gel electrophoresis, transferred to polyvinylidene fluoride membranes (Millipore, Watford, UK) and subsequently probed using the antibodies described in Supplementary Table S3, all essentially as previously described [16]. Visualisation was undertaken using HRP-conjugated secondary antibodies (Dako; used at 1:1000 dilution) and Immobilon Western Chemiluminescent HRP Substrate (Merck Millipore) and subsequent quantification was performed using Fiji [27].

2.9. Micro-computed tomography (µCT)

After mice were sacrificed by cervical dislocation, their right hind legs were fixed overnight in 10% (w/v) neutral-buffered formalin (Sigma-Aldrich) before transfer to 70% (v/v) ethanol. Limbs were analysed by µCT to examine calcified tissues using a SkyScan 1272 (Bruker, Belgium; 0.5 mm aluminium filter, 50 kV, 200 µA). Two scans were performed. Cortical bone was scanned at a voxel size of 9.0 µm, with a 0.5° rotation angle. Trabecular bone was scanned at a voxel size of 4.5 µm

using a 0.3° rotation angle. NRecon (Bruker) and DataViewer (Bruker) were used to construct cross-sectional slices or to generate 3D computational models, respectively. CTAn (Bruker) was used to quantify metrics, essentially as previously described [28]. For trabecular tibial and femoral measurements, a volume of interest (VOI) encompassing the region 90-990 µm below or above (respectively) the growth plates were used. For measuring tibial cortical bone, a VOI positioned 450-1350 µm above the point at which the fibula and tibia merge was analysed, whereas for femoral bone, a 900 µm VOI at the vertical midpoint of the femur was analysed. The bowing of the leg bones, the horizontal distance between the fibula and tibia at the midpoint of the tibia (calculated at the exact vertical midpoint between the tibial plateau and the point at which the fibula joins the tibia) was measured on the transaxial plane. Bone tissue mineral density (TMD) was calculated from cortical scans using CtAn, calibrated against phantom rods of known calcium hydroxyapatite densities of 0.25 and 0.75 g·cm⁻³ (Bruker).

2.10. Histology and histomorphometry

Mice underwent intraperitoneal injections (0.1 ml/10 g body weight) of alizarin red-S (3 mg/ml) and then calcein (2 mg/ml) 7 and 1 day prior to sacrifice. After analysis by µCT (above), the tibiae were embedded in methyl methacrylate (MMA) and 5 µm sections cut with a tungsten steel knife on a motorised rotary microtome (Leica). Sections were stained either with Goldner's Trichrome to analyse osteoid and lipid droplets or counterstained with calcein blue to quantify the amount of bone formed between the injected alazarin red-S and calcein, essentially as previously described [28]. Images were captured using an Axioscan Z1 slide scanner (Zeiss) and histomorphometry performed using the OsteoidHisto and CalceinHisto open-source image analysis programs [29]. A mean average of 3 sections/mouse was used to represent N = 1.

2.11. Three-point break testing of murine bone

Destructive three-point bend tests were carried out on the tibiae and femurs of 20-week-old mice using a CellScale Tester (UniVert), with the compression mode and 3-point bend setup. Bones were placed on 2 plinths, 8 mm apart and force applied to the centre of the bone. Force magnitude parameters used were as follows: displacement control mode for compression, with ramp function and stretch magnitude of 3mm for 30 seconds, no rest duration and no preload. Force (N) and displacement (mm) measurements were obtained every 100 milliseconds. Raw data was used to plot force displacement graphs. Stiffness (Nmm⁻¹) was defined as $\frac{\Delta \text{Force}}{\Delta \text{Displacement}}$. Maximum load was defined as the peak of the force displacement graph. Student's two-sided *t*-tests were used to assess statistical significance of each parameter between genotypes.

2.12. Osteoblast and stromal cell isolation and culture

Osteoblasts were isolated from the calvariae of 3–5-day old mouse pups essentially as previously described [28]. Briefly, dissected calvariae were digested with collagenase type I (Sigma-Aldrich) and the isolated cells cultured in α-MEM (Gibco) supplemented with 2 mM L-glutamine, 10% FBS, and antibiotics. A separate population of osteoblasts and stromal cells were isolated from femoral bone fragments (approximately 2 mm²) and marrow respectively, dissected from 20-week-old mice. The epiphyses were removed to expose the marrow, which was flushed from the bones by centrifugation and cultured directly with α-MEM (supplemented as above but also with 100 ng/ml M-CSF for 3 days to obtain M-CSF-dependent bone marrow macrophages (BMMs) [28]). The remaining bone was cut into small fragments of approximately 2 mm² and collagenase digested for 1 hour. Subsequently, the

bone chips were washed with PBS and cultured in supplemented α -MEM for approximately 6 weeks until semi-confluent layers of osteoblasts were present. Osteocytes were also isolated from bone chips, as previously described [30].

2.13. Osteoblast proliferation and alkaline phosphatase assays

For cell proliferation and alkaline phosphatase assays, osteoblasts were cultured in complete DMEM for 24 hours. Proliferation was quantified after 2.5 hours culture with Alamar Blue (ThermoFisher Scientific) following the manufacturers protocol. For alkaline phosphatase assays the cells were formalin-fixed, freeze-thawed and incubated with 20mM paranitrophenyl phosphate (PNPP) (ThermoFisher Scientific) which is dephosphorylated by alkaline phosphatase to produced paranitrophenol (PNP), the absorbance of which was measured at 405 nm after 30 minutes. PNP levels were normalised against cell proliferation measurements, all essentially as described [28].

2.14. Osteogenesis assays and alizarin red-S staining in murine osteoblasts

Osteoblasts underwent alizarin red-S staining, adapted from previously described methodology [28]. Briefly, cells were cultured in osteogenic medium (α -MEM-complete, supplemented with 2 mM β -glycerophosphate (BGP) and 50 μ g/ml L-ascorbic acid (both Sigma-Aldrich)). Calvariae and bone-chip osteoblasts were incubated for 7 days or 18 days, respectively, before being formalin-fixed, stained with 40 mM alizarin red-S for 30 minutes and imaged with an Axiovert 200 Inverted microscope (Zeiss). The alizarin red-S was extracted using 10% (w/v) cetylpyridinium chloride, the absorbance of which was measured 562 nm. Parallel cell cultures were either lysed for protein or RNA using previously described methods.

2.15. miR-324 titration and reintroduction in miR-324-null osteoblasts

miR-324-null and WT calvarial osteoblasts were isolated and cultured as described earlier. miR-324-null osteoblasts were transfected (DharmaFECT 1) with both mimics of arms of miR-324 (i.e. -5p and -3p) at final concentration ranging from 5 nM to 5 pM for 24 hours (Supplementary Figure S1), and subsequently stimulated with osteogenic media for 7 days. Cells transfected with miRIDIAN microRNA Mimic Negative Control #2 (miCon; Horizon Discovery) were included as a negative control and WT osteoblasts as a positive control. RT-qPCR for miR-324-5p and -3p was undertaken as described. Optimal concentration was determined as the level equivalent to the WT osteoblasts and was used to transfet further cultures of miR-null osteoblasts for which gene expression analysis and alizarin red-S staining were undertaken after 7 days of stimulation with osteogenic media (as described above).

2.16. Osteoclastogenesis assays and TRAP staining

M-CSF-dependent BMMs were cultured in α -MEM-complete, supplemented with 50 ng/ml RANK-L and 30 ng/ml M-CSF (Peprotech) to stimulate osteoclastogenesis. Equivalent BMM control cultures were stimulated with just M-CSF. After 5 days, RNA was extracted, or cells were fixed for Tartrate-resistant acid phosphatase (TRAP) staining. For TRAP staining, cells were formalin-fixed and assayed using the Acid Phosphatase, Leukocyte (TRAP) Kit (Sigma-Aldrich) following the manufacturer's instructions. Cells were imaged with an Axiovert 200 inverted microscope (Zeiss) and TRAP-positive cells (with ≥ 3 nuclei) in each sample were counted in addition to the number of nuclei in each of these cells. Fiji [27] was used to measure the total area covered by TRAP-positive cells with ≥ 3 nuclei, allowing calculation of the mean osteoclast area. All osteoclastogenesis assays were performed in

triplicate and the mean of the triplicates was treated as $N = 1$ for each mouse from which cells were isolated.

2.17. Adipo-osteogenesis in murine C3H10T1/2 mesenchymal stromal cells

Adipo-osteogenesis (AdiOst) co-differentiation assays were undertaken using murine C3H10T1/2 cells. Cells were transfected with either 50nM microRNA Hairpin Inhibitor Negative Control #1 (hpCon), hp-miR-324-5p hp-miR-324-3p, miCon, miR-324-5p mimic, miR-324-3p mimic (all Horizon Discovery) using DharmaFECT 1, or with the plasmids pCMV-ENTRY-*Runx2* or pCMV-ENTRY-neg using FuGene HD. 24 hours post-transfection cells were stimulated with AdiOst co-differentiation media (α -MEM-complete supplemented with 100 nM dexamethasone, 2 mM BGP and 50 μ g/ml L-ascorbic acid [28, 31]) for 18 days. From the experimental wells, either protein or RNA (Cells-to-cDNA II Kit) was extracted or the cells were stained with alizarin red-S (as described earlier) or oil red-O, undertaken as previously described [32]. Following oil red-O staining, cells were washed, imaged with an Axiovert 200 inverted microscope (Zeiss), and destained using 100% (v/v) isopropanol. The stain intensity was quantified by measuring the absorbance at 500 nm.

2.18. Statistical analysis

Unless indicated, the Shapiro-Wilk test was used to assess normality of data. Statistical significance was assessed using Student's two-tailed *t*-test (all unpaired unless indicated otherwise) for single comparisons or analysis of variance (ANOVA) for testing the effects of multiple variables on a continuous variable output; the test used for each comparison is indicated in the corresponding figure legend. All data analysis and statistical calculations were performed using R version 3.6.2 [33]. Relevant R packages used for statistical analysis are cited.

2.19. Data availability

RNA-seq data is publicly available at the NCBI Gene Expression Omnibus under the accession GSE226615.

3. Results

3.1. miR-324-null mice display a high bone mass phenotype

Human serum levels of miR-324-3p show positive correlation with bone mineral density (BMD), mineral apposition rate (MAR), bone formation rate (BFR) and mineralised bone surface [9-11]. Although most abundantly expressed in brain, miR-324 is also relatively highly expressed in bone, especially when compared to cartilage chondrocytes ([34], Supplementary Figure 2). Interestingly, the abundance of both arms of miR-324 (i.e., -5 and -3p) are generally similar, suggesting both may be functional in terms of repressing gene expression [35]. Having previously generated a miR-324-null mouse [16], we therefore sought to examine these mice for any skeletal phenotype.

Through the utilisation of micro-computed tomography (μ CT), we assessed whether the bone microstructure of male miR-324-null mice differed from WT mice, aged 5-, 7- and 14-months. Although miR-324-null mice had no obvious alterations to limb development, body size (data not shown), or limb length (Supplementary Figure S3), they did display increased bone thickness, both in the femoral and tibial trabeculae and cortex (Figure 1a and b; Supplementary Figure 4a and b). Although trabecular bone thickness remained increased in miR-324-null samples, even at 14-months, the increase in miR-324-null cortical thickness reduced with age (Figure 1b, Supplemental Figure S4 and S5, Supplemental Table S4). Overall trabecular number between genotypes approached, but was not, statistically significantly different (Supplementary Figure S6)

In addition to the miR-324-null increased bone thickness phenotype, the trabecular structural model index (SMI) significantly increased overall in both femoral and tibial miR-324-null bones (Figure 1b and Supplementary Figure S4b), suggestive of more rod-like trabeculae in the null mice and therefore a less mechanically competent structure [36]. The SMI increased with age in both genotypes of our mice, in line with ageing humans [37], therefore the miR-324-null mice may display an accelerated ageing phenotype with respect to bone. The bone tissue mineral density (TMD) of miR-324-null mice also increased in both the femur and tibia (Figure 1b, Supplementary Figure S4b and Supplementary Table S4). In both trabecular and cortical bone this increase was most apparent at the 5-month time point. Due to the observed early increase in TMD, we also investigated whether any bowing could be observed in the tibiae of miR-324-null mice, by measuring the distance between the fibula and tibia at the vertical tibial midpoint. This was indeed approximately 5% larger in the null mice, indicating increased bowing (Supplementary Figure S7). Three-point break testing of 5-month miR-324-null and WT mouse limbs revealed that the maximum tibial displacement was significantly reduced in miR-324-null samples. However, the maximum load in both tibia and femur was significantly greater in miR-324-null samples and the stiffness was also significantly increased in miR-324-null tibiae, though not in the femur (Figure 1c, Supplemental Table S4). This therefore suggested that the increased bowing observed in miR-324-null tibiae was not due to increased displacement, but instead potentially the result of altered bone remodelling.

Considering the high bone mass phenotype observed in miR-324-null mice and the suggestion of altered bone remodelling activity posited by the three-point break test results, we proceeded to investigate whether this could be explained by increased osteoblast-mediated bone formation. To assess the rate of bone formation differing between genotypes, 7- and 14-month-old mice were injected with alizarin red-S followed by calcein and bones examined histologically. This revealed an increased mineral apposition rate (MAR) and area of mineralising surface in 14-month miR-324-null

mice, as well as a significantly increased bone formation rate (BFR) at both ages (Supplemental Table S5).

Additionally, Goldner's Trichrome staining revealed that miR-324-null mice had thickened osteoid, the non-mineralised component of bone, at both ages examined (Figure 2a). The miR-324-null tibial sections also displayed a reduction in lipid droplets, both in terms of their number and mean area, although lipid droplet area reduction was not statistically significant in the 7-month cohort (Figure 2b, and Supplemental Figure S8, and Table S5). Combined, these results suggest that lack of *Mir324* in mice results in the observed high bone mass phenotype at least in part through modulating the balance between osteogenesis and adipogenesis.

3.2. miR-324-null osteoblasts display increased bone formation *ex vivo*

Since *in vivo* miR-324-null samples displayed evidence of increased bone formation, we next examined the phenotype of isolated and cultured murine calvariae pre-osteoblasts *ex vivo*. Confluent cultures of isolated cells were stimulated with osteogenic media (for 7 days), before staining with alizarin red-S or assessment for alkaline phosphatase activity. miR-324-null osteoblasts showed a statistically significant increase in both alizarin red-S intensity and alkaline phosphatase activity. Gene expression analysis of parallel cultures showed upregulation in miR-324-null osteoblasts of key osteogenesis-related genes *Alpl*, *Col1a1*, *Col1a2* and *Runx2* (Figure 3a). To confirm that the alterations in *ex vivo* mineralisation and gene expression were a consequence of miR-324 removal, both the -5p and 3p arms of the miRNA were reintroduced into miR-324-null osteoblasts, at predetermined endogenous levels (Supplementary Figure S1). Upon transfection with the mimics the increased alizarin red-S staining previously observed in miR-324-null osteoblasts was significantly reduced. Concomitantly, the expression of *Col1a2* and *Runx2* were significantly reduced, whilst the reduction of *Col1a1* expression approached significance (*p*-value = 0.054). The addition of the miR-324 mimics did not alter *Alpl* expression (Figures 3bi and 3bii).

To identify the origin of the abnormal bone formation in the osteoblasts of miR-324-null mice, osteoblasts were isolated from femoral bones of 20-week-old miR-324-null and WT mice and cultured to confluence prior to stimulation with osteogenic media for 18 days (Supplementary Figure S9). RNA-seq was subsequently undertaken, revealing that more than 3500 genes as significantly differentially expressed (adjusted *p*-value ≤ 0.05) between the genotypes (Figure 3c and Supplementary Table S6), with PCA revealing clear segregation of the samples (Figure 3d). As observed in the *ex vivo* calvarial osteoblasts, osteogenic genes *Col1a1* and *Runx2* were amongst the significantly upregulated genes. Differentially expressed genes enriched for various Disease Ontology terms, including "Arthritis" and "Rheumatoid arthritis". Gene Ontology analysis of the filtered (fold change 1.5, adjusted *p*-value < 0.05) up-regulated genes included enriched terms such as "Skeletal System Development", while down-regulated genes were present in immune related pathways (Supplementary Figure S10). Together these results demonstrate that the transcriptome of miR-324-null osteoblasts is distinct from that of WT osteoblasts.

3.3. *Runx2* is a direct target of miR-324-5p in osteoblasts

To elucidate direct targets of miR-324 regulated in the osteoblast data, the 1,596 significantly upregulated genes were filtered to include those known to have an impact on bone- or metabolism-related disorders using Disease Ontology [24] (Supplementary Table S2, Figure 4a). These were

subsequently filtered using the TargetScan miRNA target prediction algorithm, resulting in the selection of four osteoblast putative miR-324 target genes; *Klf7*, *Cxcl12* (which encodes SDF-1), *Top1* and *Runx2* (Figure 4b), for validation in 3'UTR-luciferase assays (Supplemental Table S7). Multiple *Cxcl12* 3'UTR-luciferase reporters were generated since the murine gene can be one of 3 discrete isoforms, *Cxcl12-α*, *Cxcl12-β* and *Cxcl12-γ*, none of which share an identical 3'UTR or all of the same miR-324-5p or -3p predicted binding sites (Supplementary Figure S11) and all were upregulated in the miR-324-null osteoblasts. *Cxcl12-α* is the canonical isoform [38]. Transfection of the immortalised murine MSC-like cell line C3H10T1/2 with the reporters identified that only the *Runx2* and *Cxcl12-γ* 3'UTRs displayed significant repression of the upstream luciferase gene when miR-324-5p (for *Runx2*), or miR-324-5p and -3p (for *Cxcl12-γ*) were individually co-transfected (Figures 4c and 4d). Since the other *Cxcl12* 3'UTR-luciferase reporters were not repressed by miR-324 we hypothesised that miR-324-5p and -3p were targeting *Cxcl12-γ* at sites unique to this 3'UTR, although the predicted miR-324-3p binding site within this sequence was only predicted by miRmap [25], not TargetScan. Indeed a 3'UTR-luciferase reporter of just the unique *Cxcl12-γ* 3'UTR sequence was repressed by both miR-324-5p and miR-324-3p. The miR-324-mediated repression of both *Runx2* and *Cxcl12-γ* (unique) were abolished when 2 nucleotides in each miR-324 binding site were mutated (Figures 4c, 4d, and Supplemental Table S7), therefore these genes are likely novel, previously unpublished, targets of the miRNA.

3.4. miR-324-5p and *Runx2* regulate the balance between osteogenesis and adipogenesis

Both *in vivo* and *ex vivo*, miR-324-null samples showed increased bone formation and *in vivo* reduced lipid droplets within the tibial bone marrow. Considering these results and that we identified *Runx2*, an essential osteogenic transcription factor, as a direct miR-324-5p target, we hypothesised that the miR-324-null high bone mass and reduced lipid phenotypes were driven directly by *Runx2* dysregulation. To investigate the mechanism of altered osteogenesis and adipogenesis, we transfected C3H10T1/2 cells with miR-324-5p miRNA mimic or hairpin (hp-) inhibitor and stimulated osteogenesis and adipogenesis using co-differentiation (AdiOst) medium [31]. After 14 days of stimulation parallel cell cultures were stained with alizarin red-S or oil red-O staining, for mineralisation and fat deposits, respectively, and the ratio of staining intensity determined. Inhibition of miR-324-5p significantly increased osteogenesis whilst inhibiting adipogenesis, and the converse was true with the miR-324-5p mimic (Figure 5a). Mechanistically, inhibition of the miRNA increased expression of *Runx2* but decreased *Pparg*, a regulator of adipocyte differentiation. The miRNA mimic caused an increase in the expression of *Pparg* (Figure 5b). Indeed, overexpression of *Runx2* alone (Figure 5c) recapitulated these results, increasing osteogenesis at the expense of adipogenesis, with samples showing a decrease in *Pparg* expression (Figures 5d and e). Overall, these results phenocopy the *in vivo* data and imply that much of the action of miR-324 on osteogenesis occurs through the repressive effect it exerts on *Runx2*.

3.5. The osteoclast and bone marrow macrophage transcriptomes are severely modulated in miR-324-null mice

In vivo, osteoblast-mediated bone formation is balanced by osteoclast-mediated bone resorption in healthy individuals. Therefore, the abundance of osteoclasts was also investigated, as the activity of these cells may also be regulated by miR-324. Seven- and 14-month miR-324-null tibiae were stained

for Tartrate-resistant acid phosphatase (TRAP), a key osteoclast marker. This revealed that the mean number of osteoclasts per bone volume was statistically significantly reduced in miR-324-null mice (Figure 6a). The osteoclast surface area per bone surface area was also reduced, although not significantly. These results in tandem with the increased bone formation suggest that the high bone mass phenotype in miR-324-null mice may be due to both reduced bone resorption and increased bone formation. To investigate whether this effect could be replicated *ex vivo*, stromal cells were isolated from miR-324-null and WT bone marrow and stimulated with M-CSF to produce bone marrow macrophages (BMMs) and subsequently with M-CSF and RANK-L to induce osteoclastogenesis. TRAP staining of the osteoclast cultures revealed that the lack of miR-324 resulted in fewer osteoclasts, a reduced osteoclast area and fewer nuclei per osteoclast (Figure 6b).

To identify the basis of this osteoclastogenic inhibition, RNA-seq was undertaken in the miR-324-null and WT HSC-differentiate osteoclasts (Supplemental Table S6). At a transcriptomic level, miR-324-null osteoclasts were highly distinct from WT osteoclasts; remarkably a total of 8865 genes were differentially expressed between genotypes (43% of all genes detected). This implies that the lack of osteoclastogenesis in miR-324-null samples is probably due to a defect in BMMs or HSCs prior to osteoclast differentiation. In light of this we conducted RNA-seq of miR-324-null and WT BMMs (HSCs stimulated with only M-CSF), in which a total of 7021 genes were significantly differentially expressed in miR-324-null BMMs relative to WT controls (Figure 6c). Notably, the most highly defined cell type using the transcriptomic data from both miR-324-null and WT BMMs was “Macrophages”. In the WT osteoclast transcriptomic data “Osteoclasts” was the most highly defined cell type, whereas in miR-324-null osteoclasts this remained as “Macrophages” (Supplementary Table S8). In both experiments, samples segregated by genotype on PCA (Figure 6d). Of note, included in the significantly down-regulated genes in both data sets were *Nfatc1* and *Tnfrsf11a*, the genes encoding the key osteoclastogenesis transcription factor and the RANK receptor, respectively [40, 41]. Several pathways relevant to osteoclastogenesis were also enriched within the datasets (Supplementary Figure S12a). Interestingly, *Acp5*, which encodes TRAP, and *Mmp9* were downregulated in miR-324-null osteoclasts yet upregulated in the BMMs (Supplementary Figure S12b). The majority of genes dysregulated in both cell types were dysregulated in the same direction in both BMMs and osteoclasts (Supplementary Figure S13).

We next attempted to identify targets in the BMMs, since there were fewer significantly differentially expressed genes. In all, 3700 genes were significantly upregulated (adjusted p-value ≤ 0.05 and $\log_2\text{FC} > 0$). Using the same target prediction pipeline as for the osteoblast dataset, 42 bone or metabolism disease-associated putative miR-324 targets were significantly upregulated in the BMM dataset (Figure 7a), of which 9 passed the thresholds for the TargetScan total context score and the \log_2 fold-change (< -0.25 and > 0.35 , respectively); *Ccne1*, *Pdgfa*, *Klf7*, *Icam1*, *Bcl2*, *Pin1*, *Ing1*, *Ptgs1* and *App* (Figure 7b). 3'UTR luciferase reporter analysis of each of these genes revealed that *Pdgfa*, *Pin1*, *Ptgs1* and *App* were direct miR-324 targets (Figure 7c), with mutated miR-324 seed-sequences relieving the miRNA mediated repression (Figure 7d and Supplemental Table S7). Three of these 4 miR-324 target genes have been implicated in the process of osteoclastogenesis [42-45] and therefore may partially explain the consequences of miR-324 loss on osteoclast differentiation. All four genes are novel validated targets of miR-324. Human *PIN1* and *PTGS1* have limited

experimentally-validation as miR-324-5p and miR-324-3p targets respectively [46], the alternate miRNA arms to the data herein.

4. Discussion

Having developed the first miR-324-null mouse [16], we investigated any bone phenotype of these animals, since the miRNA has been associated with bone disease, including bone formation and as a serum marker for fracture risk [9-12]. From our analysis the mice lacking the *Mir324* locus had an increase in trabecular and cortical thickness. The trabecular differences were evident through all the ages of mice analysed, however cortical bone parameters between the genotypes somewhat normalised with age. Overall, our data indicated that the bone differences likely manifested through both reduced osteoclastogenesis and increased bone formation. This was further supported by the observation that although miR-324-null mice display increased tibial bowing, they in fact had significantly reduced maximum tibial displacement upon three-point break testing, pointing to a defect in bone remodelling rather than a reduction in stiffness. A major limitation of the work herein is the focus on male only mice for the μ CT data, though for other experiments both sexes were utilised. Clearly the bone structure of female miR-324-null mice requires analysis.

Numerous studies have described the importance of miRNAs in bone formation and homeostasis [47]. The conditional deletion of miRNA species by removal of the miRNA processing enzyme Dicer in osteoblasts or osteoclasts result in mice with increased bone mass [48-50], however this phenotype is somewhat timing and Cre-driver dependent [47]. Whilst it is not uncommon for a miRNA to affect a component of skeletal biology [47, 51, 52], it is unusual for more than one component of bone remodelling to be altered. However, some miRNAs may affect more than one cell-type in bone. Osteoclast-specific deletion of miR-182 increases post-natal trabecular bone mass [53], while (in zebrafish) the miRNA suppresses osteoblast differentiation [54]. miR-21 enhances both osteogenesis and osteoclastogenesis *in vitro* [55, 56], however bone phenotype of the mice is due to dysregulated osteoclast activity as opposed to osteoblast-mediated bone formation. Our data shows that uniquely the loss of miR-324 consistently affects both osteoblasts and osteoclasts *in vivo*, *in vitro* or *ex vivo*.

Perhaps contrary to our murine observations, a positive correlation has been identified between human miR-324-3p serum abundance and BMD, with miR-324 contributing to a group of 8 miRNAs that can be used as a discriminator between controls and patients with low-traumatic fractures [10]. However, these measurements were obtained from human serum and therefore the cellular origin of these serum miRNAs are unclear. A possible explanation for the discordance with our data is that miR-324 is secreted from cells because of its ability to repress bone formation, although this hypothesis requires further investigation.

miR-324-null mice present with an osteoclast deficiency *in vivo* and impaired osteoclastogenesis *ex vivo*. Over 40% of all genes tested were significantly dysregulated in *ex vivo* miR-324-null osteoclasts (adjusted p-value ≤ 0.05) and more than half of these were also dysregulated even in BMMs, suggesting the defect is present earlier in the haematopoietic lineage. Conditional deletion of *Dicer* in hematopoietic progenitor cells confirms that miRNAs play a role in haematopoiesis, including specific miRNAs, such as miR-125a [57]. The evaluation of miR-324 loss in haematopoiesis would therefore be of interest but could be indirect, since adipocyte-derived lipids found in bone marrow have a supportive role in HSC proliferation [58], reportedly via adipocyte-secreted factors such as adiponectin and leptin [59-61]. We observed decreased *in vitro* adipogenesis and the reduced *in vivo*

bone marrow lipid accumulation following miR-324 deletion. We propose this is in part due to the upregulation of miR-324-5p target gene *Runx2*, skewing cell differentiation, at least in our simplistic AdiOst assays. However, we also identified *Cxcl12-γ* as a direct of both arms of miR-324. Bone marrow stromal cells provide support for hematopoietic cells and are the source of osteoblasts. They can also express *Cxcl12*, termed CXCL12-abundant (CAR) cells [62-64], which contain recently defined subpopulations 'Adipo-CAR' and 'Osteo-CAR' cells [65], with differing, not yet fully defined, functions within the bone marrow, including transformation to osteoblasts upon bone injury [66]. Deletion of *CXCL12* from Adipo-CAR leads to extensive marrow adipogenesis in adult bone marrow via conversion of these cells to lipid-laden marrow adipocytes and reduced stromal-haematopoiesis [67]. Given our observation that miR-324 targets *Cxcl12-γ*, examining CAR-cell populations within the marrow of null mice would clearly be of interest.

An interesting parallel can be observed between the miR-324-null phenotype and that of sclerostin (*Sost*)-null mice [68]. In both, bone formation is increased although is notably greater in the *Sost*-null mice; trabecular thickness is increased by 12% in 5-month-old male miR-324-null mice but by 146% in equivalent *Sost*-null animals. Sclerostin is secreted by osteocytes and negatively regulates canonical Wnt signalling pathways to suppress osteogenesis, with anti-sclerostin therapy, Romosozumab, an approved treatment of some-types of osteoporosis [69]. The Gene Ontology term "Wnt signalling" pathway was significantly enriched in the miR-324-null osteoblast transcriptomic data (adjusted p-value = 7.81×10^{-3}), due to upregulation of genes such as *Sox9* and *Wnt6* (adjusted p-values = 8.61×10^{-5} and 2.90×10^{-5} , respectively). Considering the parallels in phenotype and affected pathways between miR-324-null and *Sost*-null mice, osteocyte function should be examined in our miR-324-null mice. Sclerostin modulates the RANKL/RANK/OPG pathway, which is central to bone homeostasis. Serum levels of RANKL and OPG in the miR-324 mouse would also be worthy of measurement.

In summary, we showed that miR-324-null mice displayed an increase in bone mass, with trabecular differences exacerbated or maintained with age, while cortical bone differences somewhat normalised. The mice have fewer adipocyte-derived lipid droplets and osteoclasts, while having an increased activity of osteoblasts. Indeed, the increase in osteoblast function we attribute to up-regulation of *Runx2*, identified here as a novel miR-324-5p target, but is likely the result of dysregulation of multiple targets and pathways. These data also suggest miR-324 is an important driver of SSC commitment to the adipocyte lineage. Perhaps most strikingly, deletion of miR-324 causes a dramatic transcriptome alteration in *ex vivo* cultured macrophages and resultant osteoclasts. Further work is required to determine how and when miR-324 functions during haematopoiesis. However, these phenotypes have posited miR-324 as a novel pharmaceutical target which regulates bone diseases through osteoblasts, osteoclasts and, through the modulation of mesenchymal lineage commitment, adipocytes (summarised in Figure 8).

The age-related disease osteoporosis negatively affects both cortical and trabecular bone. Our data suggests inhibition of miR-324 offers some promise for the treatment of the disease, perhaps more so for the trabecular changes observed. A deeper understanding of the regulatory role of miR-324 in bone and the musculoskeletal system as a whole is required prior to development of such a treatment, and therefore this should form the basis of future research.

Funding

For the purpose of open access, the author has applied a Creative Commons Attribution (CC BY) licence to any Author Accepted Manuscript version arising from this submission. This work was supported by the Medical Research Council and Versus Arthritis as part of the MRC-Arthritis Research UK Centre for Integrated Research into Musculoskeletal Ageing (CIMA) [JXR 10641, MR/P020941/1]; The Dunhill Medical Trust [R476/0516]; Versus Arthritis [19424, 22043]; the JGW Patterson Foundation; and the NIHR Newcastle Biomedical Research.

Conflicts of Interest

All authors declare no conflicts of interest.

Contributions

DAY, IMC, MJB, DJH and RVH conceived and designed the work that led to the submission. DJH, HL, AP, GC, YH, RDP and MJB acquired data. DJH, FJSB, RDP, JS, KAP, MJP, RVH and DAY interpreted the results. DJH, DAY, FJSB, RDP and RVH drafted or revised the manuscript. All authors approved the final manuscript.

References

- [1] B.P. Lewis, C.B. Burge, D.P. Bartel, Conserved seed pairing, often flanked by adenosines, indicates that thousands of human genes are microRNA targets, *Cell* 120(1) (2005) 15-20. 10.1016/j.cell.2004.12.035
- [2] R.F. Loeser, S.R. Goldring, C.R. Scanzello, M.B. Goldring, Osteoarthritis: a disease of the joint as an organ, *Arthritis Rheum* 64(6) (2012) 1697-707. 10.1002/art.34453
- [3] T. Vilaca, R. Eastell, M. Schini, Osteoporosis in men, *Lancet Diabetes Endocrinol* 10(4) (2022) 273-283. 10.1016/S2213-8587(22)00012-2
- [4] U.H. Lerner, Bone remodeling in post-menopausal osteoporosis, *J Dent Res* 85(7) (2006) 584-95. 10.1177/154405910608500703
- [5] A. Salhotra, H.N. Shah, B. Levi, M.T. Longaker, Mechanisms of bone development and repair, *Nat Rev Mol Cell Biol* 21(11) (2020) 696-711. 10.1038/s41580-020-00279-w
- [6] M. Puppo, H. Taipaleenmaki, E. Hesse, P. Clezardin, Non-coding RNAs in bone remodelling and bone metastasis: Mechanisms of action and translational relevance, *Br J Pharmacol* 178(9) (2021) 1936-1954. 10.1111/bph.14836
- [7] Q. Cui, J. Xing, M. Yu, Y. Wang, J. Xu, Y. Gu, X. Nan, W. Ma, H. Liu, H. Zhao, Mmu-miR-185 depletion promotes osteogenic differentiation and suppresses bone loss in osteoporosis through the Bgn-mediated BMP/Smad pathway, *Cell Death Dis* 10(3) (2019) 172. 10.1038/s41419-019-1428-1

[8] Y. Lee, H.J. Kim, C.K. Park, Y.G. Kim, H.J. Lee, J.Y. Kim, H.H. Kim, MicroRNA-124 regulates osteoclast differentiation, *Bone* 56(2) (2013) 383-9. 10.1016/j.bone.2013.07.007

[9] X. Feichtinger, C. Muschitz, P. Heimel, A. Baierl, A. Fahrleitner-Pammer, H. Redl, H. Resch, E. Geiger, S. Skalicky, R. Dormann, F. Plachet, P. Pietschmann, J. Grillari, M. Hackl, R. Kocjan, Bone-related Circulating MicroRNAs miR-29b-3p, miR-550a-3p, and miR-324-3p and their Association to Bone Microstructure and Histomorphometry, *Sci Rep* 8(1) (2018) 4867. 10.1038/s41598-018-22844-2

[10] R. Kocjan, C. Muschitz, E. Geiger, S. Skalicky, A. Baierl, R. Dormann, F. Plachet, X. Feichtinger, P. Heimel, A. Fahrleitner-Pammer, J. Grillari, H. Redl, H. Resch, M. Hackl, Circulating microRNA Signatures in Patients With Idiopathic and Postmenopausal Osteoporosis and Fragility Fractures, *J Clin Endocrinol Metab* 101(11) (2016) 4125-4134. 10.1210/jc.2016-2365

[11] S. Weilner, S. Skalicky, B. Salzer, V. Keider, M. Wagner, F. Hildner, C. Gabriel, P. Dovjak, P. Pietschmann, R. Grillari-Voglauer, J. Grillari, M. Hackl, Differentially circulating miRNAs after recent osteoporotic fractures can influence osteogenic differentiation, *Bone* 79 (2015) 43-51. 10.1016/j.bone.2015.05.027

[12] S. Woods, M.J. Barter, H.R. Elliott, C.M. McGillivray, M.A. Birch, I.M. Clark, D.A. Young, miR-324-5p is up regulated in end-stage osteoarthritis and regulates Indian Hedgehog signalling by differing mechanisms in human and mouse, *Matrix Biol* 77 (2019) 87-100. 10.1016/j.matbio.2018.08.009

[13] E. Ferretti, E. De Smaele, E. Miele, P. Laneve, A. Po, M. Pelloni, A. Paganelli, L. Di Marcotullio, E. Caffarelli, I. Scrpanti, I. Bozzoni, A. Gulino, Concerted microRNA control of Hedgehog signalling in cerebellar neuronal progenitor and tumour cells, *EMBO J.* 27(19) (2008) 2616-2627. 10.1038/emboj.2008.172

[14] H.S. Xu, H.L. Zong, M. Shang, X. Ming, J.P. Zhao, C. Ma, L. Cao, MiR-324-5p inhibits proliferation of glioma by target regulation of GLI1, *Eur. Rev. Med. Pharmacol. Sci.* 18(6) (2014) 828-832.

[15] L.P. Lai, J. Mitchell, Indian hedgehog: its roles and regulation in endochondral bone development, *J. Cell. Biochem.* 96(6) (2005) 1163-1173. 10.1002/jcb.20635

[16] D.J. Hayman, T. Modebadze, S. Charlton, K. Cheung, J. Soul, H. Lin, Y. Hao, C.G. Miles, D. Tsompani, R.M. Jackson, M.D. Briggs, K.A. Pirog, I.M. Clark, M.J. Barter, G.J. Clowry, F.E.N. LeBeau, D.A. Young, Increased hippocampal excitability in miR-324-null mice, *Sci Rep* 11(1) (2021) 10452. 10.1038/s41598-021-89874-1

[17] M.J. Barter, W. Hui, R.L. Lakey, J.B. Catterall, T.E. Cawston, D.A. Young, Lipophilic statins prevent matrix metalloproteinase-mediated cartilage collagen breakdown by inhibiting protein geranylgeranylation, *Ann Rheum Dis* 69(12) (2010) 2189-98. 10.1136/ard.2010.129197

[18] N.L. Bray, H. Pimentel, P. Melsted, L. Pachter, Near-optimal probabilistic RNA-seq quantification, *Nat Biotechnol* 34(5) (2016) 525-7. 10.1038/nbt.3519

[19] D.M. Church, L. Goodstadt, L.W. Hillier, M.C. Zody, S. Goldstein, X. She, C.J. Bult, R. Agarwala, J.L. Cherry, M. DiCuccio, W. Hlavina, Y. Kapustin, P. Meric, D. Maglott, Z. Birtle, A.C. Marques, T. Graves, S. Zhou, B. Teague, K. Potamousis, C. Churas, M. Place, J. Herschleb, R. Runnheim, D. Forrest, J. Amos-Landgraf, D.C. Schwartz, Z. Cheng, K. Lindblad-Toh, E.E. Eichler, C.P. Ponting, C. Mouse Genome Sequencing, Lineage-specific biology revealed by a finished genome assembly of the mouse, *PLoS Biol* 7(5) (2009) e1000112. 10.1371/journal.pbio.1000112

[20] C. Soneson, M.I. Love, M.D. Robinson, Differential analyses for RNA-seq: transcript-level estimates improve gene-level inferences, *F1000Res* 4 (2015) 1521. 10.12688/f1000research.7563.2

[21] M.I. Love, W. Huber, S. Anders, Moderated estimation of fold change and dispersion for RNA-seq data with DESeq2, *Genome Biol* 15(12) (2014) 550. 10.1186/s13059-014-0550-8

[22] E.Y. Chen, C.M. Tan, Y. Kou, Q. Duan, Z. Wang, G.V. Meirelles, N.R. Clark, A. Ma'ayan, Enrichr: interactive and collaborative HTML5 gene list enrichment analysis tool, *BMC Bioinformatics* 14 (2013) 128. 10.1186/1471-2105-14-128

[23] O. Franzen, L.M. Gan, J.L.M. Bjorkegren, PanglaoDB: a web server for exploration of mouse and human single-cell RNA sequencing data, *Database (Oxford)* 2019 (2019). 10.1093/database/baz046

[24] L.M. Schriml, E. Mitraka, J. Munro, B. Tauber, M. Schor, L. Nickle, V. Felix, L. Jeng, C. Bearer, R. Lichenstein, K. Bisordi, N. Campion, B. Hyman, D. Kurland, C.P. Oates, S. Kibbey, P. Sreekumar, C. Le, M. Giglio, C. Greene, Human Disease Ontology 2018 update: classification, content and workflow expansion, *Nucleic Acids Res* 47(D1) (2019) D955-D962. 10.1093/nar/gky1032

[25] C.E. Vejnar, E.M. Zdobnov, MiRmap: comprehensive prediction of microRNA target repression strength, *Nucleic Acids Res* 40(22) (2012) 11673-83. 10.1093/nar/gks901

[26] M.J. Barter, M. Tselepi, R. Gomez, S. Woods, W. Hui, G.R. Smith, D.P. Shanley, I.M. Clark, D.A. Young, Genome-Wide MicroRNA and Gene Analysis of Mesenchymal Stem Cell Chondrogenesis Identifies an Essential Role and Multiple Targets for miR-140-5p, *Stem Cells* 33(11) (2015) 3266-80. 10.1002/stem.2093

[27] J. Schindelin, I. Arganda-Carreras, E. Frise, V. Kaynig, M. Longair, T. Pietzsch, S. Preibisch, C. Rueden, S. Saalfeld, B. Schmid, J.Y. Tinevez, D.J. White, V. Hartenstein, K. Eliceiri, P. Tomancak, A. Cardona, Fiji: an open-source platform for biological-image analysis, *Nat Methods* 9(7) (2012) 676-82. 10.1038/nmeth.2019

[28] F.M. Johnson de Sousa Brito, A. Butcher, A. Pisconti, B. Poulet, A. Prior, G. Charlesworth, C. Sperinck, M. Scotto di Mase, K. Liu, G. Bou-Gharios, R. Jurgen van 't Hof, A. Daroszewska, Syndecan-3 enhances anabolic bone formation through WNT signaling, *FASEB J* 35(4) (2021) e21246. 10.1096/fj.202002024R

[29] R.J. van 't Hof, L. Rose, E. Bassonga, A. Daroszewska, Open source software for semi-automated histomorphometry of bone resorption and formation parameters, *Bone* 99 (2017) 69-79. 10.1016/j.bone.2017.03.051

[30] H. Qing, L. Ardeshirpour, P.D. Pajevic, V. Dusevich, K. Jahn, S. Kato, J. Wysolmerski, L.F. Bonewald, Demonstration of osteocytic perilacunar/canalicular remodeling in mice during lactation, *J Bone Miner Res* 27(5) (2012) 1018-29. 10.1002/jbmr.1567

[31] O. Ghali, O. Broux, G. Falgayrac, N. Haren, J.P. van Leeuwen, G. Penel, P. Hardouin, C. Chauveau, Dexamethasone in osteogenic medium strongly induces adipocyte differentiation of mouse bone marrow stromal cells and increases osteoblast differentiation, *BMC Cell Biol* 16 (2015) 9. 10.1186/s12860-015-0056-6

[32] M.J. Barter, R. Gomez, S. Hyatt, K. Cheung, A.J. Skelton, Y. Xu, I.M. Clark, D.A. Young, The long non-coding RNA ROCR contributes to SOX9 expression and chondrogenic differentiation of human mesenchymal stem cells, *Development* 144(24) (2017) 4510-4521. 10.1242/dev.152504

[33] R Core Team, A language and environment for statistical computing, R Foundation for Statistical Computing, Vienna, Austria, 2019.

[34] A. Keller, L. Groger, T. Tschernerg, J. Solomon, O. Laham, N. Schaum, V. Wagner, F. Kern, G.P. Schmartz, Y. Li, A. Borcherding, C. Meier, T. Wyss-Coray, E. Meese, T. Fehlmann, N. Ludwig, miRNATissueAtlas2: an update to the human miRNA tissue atlas, *Nucleic Acids Res* 50(D1) (2022) D211-D221. 10.1093/nar/gkab808

[35] C. Backes, T. Fehlmann, F. Kern, T. Kehl, H.P. Lenhof, E. Meese, A. Keller, miRCarta: a central repository for collecting miRNA candidates, *Nucleic Acids Research* 46(D1) (2018) D160-D167. 10.1093/nar/gkx851

[36] P.L. Salmon, C. Ohlsson, S.J. Shefelbine, M. Doube, Structure Model Index Does Not Measure Rods and Plates in Trabecular Bone, *Front Endocrinol (Lausanne)* 6 (2015) 162. 10.3389/fendo.2015.00162

[37] H. Chen, X. Zhou, H. Fujita, M. Onozuka, K.Y. Kubo, Age-related changes in trabecular and cortical bone microstructure, *Int J Endocrinol* 2013 (2013) 213234. 10.1155/2013/213234

[38] M. Janowski, Functional diversity of SDF-1 splicing variants, *Cell Adh Migr* 3(3) (2009) 243-9. 10.4161/cam.3.3.8260

[39] A. Grimson, K.K. Farh, W.K. Johnston, P. Garrett-Engele, L.P. Lim, D.P. Bartel, MicroRNA targeting specificity in mammals: determinants beyond seed pairing, *Mol Cell* 27(1) (2007) 91-105. 10.1016/j.molcel.2007.06.017

[40] Y. He, K. Staser, S.D. Rhodes, Y. Liu, X. Wu, S.J. Park, J. Yuan, X. Yang, X. Li, L. Jiang, S. Chen, F.C. Yang, Erk1 positively regulates osteoclast differentiation and bone resorptive activity, *PLoS One* 6(9) (2011) e24780. 10.1371/journal.pone.0024780

[41] K. Sato, H. Takayanagi, Osteoclasts, rheumatoid arthritis, and osteoimmunology, *Curr Opin Rheumatol* 18(4) (2006) 419-26. 10.1097/01.bor.0000231912.24740.a5

[42] S. Cui, F. Xiong, Y. Hong, J.U. Jung, X.S. Li, J.Z. Liu, R. Yan, L. Mei, X. Feng, W.C. Xiong, APPswe/Abeta regulation of osteoclast activation and RAGE expression in an age-dependent manner, *J Bone Miner Res* 26(5) (2011) 1084-98. 10.1002/jbmr.299

[43] H.H. Guo, L. Xiong, J.X. Pan, D. Lee, K. Liu, X. Ren, B. Wang, X. Yang, S. Cui, L. Mei, W.C. Xiong, Hepcidin contributes to Swedish mutant APP-induced osteoclastogenesis and trabecular bone loss, *Bone Res* 9(1) (2021) 31. 10.1038/s41413-021-00146-0

[44] R. Islam, H.S. Bae, W.J. Yoon, K.M. Woo, J.H. Baek, H.H. Kim, T. Uchida, H.M. Ryoo, Pin1 regulates osteoclast fusion through suppression of the master regulator of cell fusion DC-STAMP, *J Cell Physiol* 229(12) (2014) 2166-74. 10.1002/jcp.24679

[45] M.M. Rahman, K. Matsuoka, S. Takeshita, K. Ikeda, Secretion of PDGF isoforms during osteoclastogenesis and its modulation by anti-osteoclast drugs, *Biochem Biophys Res Commun* 462(2) (2015) 159-64. 10.1016/j.bbrc.2015.04.115

[46] H.Y. Huang, Y.C. Lin, S. Cui, Y. Huang, Y. Tang, J. Xu, J. Bao, Y. Li, J. Wen, H. Zuo, W. Wang, J. Li, J. Ni, Y. Ruan, L. Li, Y. Chen, Y. Xie, Z. Zhu, X. Cai, X. Chen, L. Yao, Y. Chen, Y. Luo, S. LuXu, M. Luo, C.M. Chiu, K. Ma, L. Zhu, G.J. Cheng, C. Bai, Y.C. Chiang, L. Wang, F. Wei, T.Y. Lee, H.D. Huang, miRTarBase update 2022: an informative resource for experimentally validated miRNA-target interactions, *Nucleic Acids Res* 50(D1) (2022) D222-D230. 10.1093/nar/gkab1079

[47] A.P. Hensley, A. McAlinden, The role of microRNAs in bone development, *Bone* 143 (2021) 115760. 10.1016/j.bone.2020.115760

[48] T. Gaur, S. Hussain, R. Mudhasani, I. Parulkar, J.L. Colby, D. Frederick, B.E. Kream, A.J. van Wijnen, J.L. Stein, G.S. Stein, S.N. Jones, J.B. Lian, Dicer inactivation in osteoprogenitor cells compromises fetal survival and bone formation, while excision in differentiated osteoblasts increases bone mass in the adult mouse, *Dev Biol* 340(1) (2010) 10-21. 10.1016/j.ydbio.2010.01.008

[49] T. Sugatani, K.A. Hruska, Impaired micro-RNA pathways diminish osteoclast differentiation and function, *J Biol Chem* 284(7) (2009) 4667-78. 10.1074/jbc.M805777200

[50] F. Mizoguchi, Y. Izu, T. Hayata, H. Hemmi, K. Nakashima, T. Nakamura, S. Kato, N. Miyasaka, Y. Ezura, M. Noda, Osteoclast-specific Dicer gene deficiency suppresses osteoclastic bone resorption, *J Cell Biochem* 109(5) (2010) 866-75. 10.1002/jcb.22228

[51] M.M. Weivoda, S.K. Lee, D.G. Monroe, miRNAs in osteoclast biology, *Bone* 143 (2021) 115757. 10.1016/j.bone.2020.115757

[52] L.I. Plotkin, J.M. Wallace, MicroRNAs and osteocytes, *Bone* 150 (2021) 115994. 10.1016/j.bone.2021.115994

[53] K. Inoue, Z. Deng, Y. Chen, E. Giannopoulou, R. Xu, S. Gong, M.B. Greenblatt, L.S. Mangala, G. Lopez-Berestein, D.G. Kirsch, A.K. Sood, L. Zhao, B. Zhao, Bone protection by inhibition of microRNA-182, *Nat Commun* 9(1) (2018) 4108. 10.1038/s41467-018-06446-0

[54] K.M. Kim, S.J. Park, S.H. Jung, E.J. Kim, G. Jogeswar, J. Ajita, Y. Rhee, C.H. Kim, S.K. Lim, miR-182 is a negative regulator of osteoblast proliferation, differentiation, and skeletogenesis through targeting FoxO1, *J Bone Miner Res* 27(8) (2012) 1669-79. 10.1002/jbmr.1604

[55] N. Yang, G. Wang, C. Hu, Y. Shi, L. Liao, S. Shi, Y. Cai, S. Cheng, X. Wang, Y. Liu, L. Tang, Y. Ding, Y. Jin, Tumor necrosis factor alpha suppresses the mesenchymal stem cell osteogenesis promoter miR-21 in estrogen deficiency-induced osteoporosis, *J Bone Miner Res* 28(3) (2013) 559-73. 10.1002/jbmr.1798

[56] T. Sugatani, J. Vacher, K.A. Hruska, A microRNA expression signature of osteoclastogenesis, *Blood* 117(13) (2011) 3648-57. 10.1182/blood-2010-10-311415

[57] S. Guo, J. Lu, R. Schlanger, H. Zhang, J.Y. Wang, M.C. Fox, L.E. Purton, H.H. Fleming, B. Cobb, M. Merkenschlager, T.R. Golub, D.T. Scadden, MicroRNA miR-125a controls hematopoietic stem cell number, *Proc Natl Acad Sci U S A* 107(32) (2010) 14229-34. 10.1073/pnas.0913574107

[58] H. Wang, Y. Leng, Y. Gong, Bone Marrow Fat and Hematopoiesis, *Front Endocrinol (Lausanne)* 9 (2018) 694. 10.3389/fendo.2018.00694

[59] Y. Umemoto, K. Tsuji, F.C. Yang, Y. Ebihara, A. Kaneko, S. Furukawa, T. Nakahata, Leptin stimulates the proliferation of murine myelocytic and primitive hematopoietic progenitor cells, *Blood* 90(9) (1997) 3438-43.

[60] B.D. Bennett, G.P. Solar, J.Q. Yuan, J. Mathias, G.R. Thomas, W. Matthews, A role for leptin and its cognate receptor in hematopoiesis, *Curr Biol* 6(9) (1996) 1170-80. 10.1016/s0960-9822(02)70684-2

[61] L. DiMascio, C. Voermans, M. Uqoezwa, A. Duncan, D. Lu, J. Wu, U. Sankar, T. Reya, Identification of adiponectin as a novel hemopoietic stem cell growth factor, *J Immunol* 178(6) (2007) 3511-20. 10.4049/jimmunol.178.6.3511

[62] Q. Zhu, L. Ding, R. Yue, Skeletal stem cells: a game changer of skeletal biology and regenerative medicine?, *Life Med* 1(3) (2022) 294-306. 10.1093/lifemedi/lnc038

[63] T. Sugiyama, H. Kohara, M. Noda, T. Nagasawa, Maintenance of the hematopoietic stem cell pool by CXCL12-CXCR4 chemokine signaling in bone marrow stromal cell niches, *Immunity* 25(6) (2006) 977-88. 10.1016/j.jimmuni.2006.10.016

[64] Y. Omatsu, T. Sugiyama, H. Kohara, G. Kondoh, N. Fujii, K. Kohno, T. Nagasawa, The essential functions of adipo-osteogenic progenitors as the hematopoietic stem and progenitor cell niche, *Immunity* 33(3) (2010) 387-99. 10.1016/j.jimmuni.2010.08.017

[65] C. Baccin, J. Al-Sabah, L. Velten, P.M. Helbling, F. Grunschlager, P. Hernandez-Malmierca, C. Nombela-Arrieta, L.M. Steinmetz, A. Trumpp, S. Haas, Combined single-cell and spatial transcriptomics reveal the molecular, cellular and spatial bone marrow niche organization, *Nat Cell Biol* 22(1) (2020) 38-48. 10.1038/s41556-019-0439-6

[66] Y. Matsushita, M. Nagata, K.M. Kozloff, J.D. Welch, K. Mizuhashi, N. Tokavanich, S.A. Hallett, D.C. Link, T. Nagasawa, W. Ono, N. Ono, A Wnt-mediated transformation of the bone marrow stromal cell identity orchestrates skeletal regeneration, *Nat Commun* 11(1) (2020) 332. 10.1038/s41467-019-14029-w

[67] Y. Matsushita, A.K.Y. Chu, W. Ono, J.D. Welch, N. Ono, Intercellular Interactions of an Adipogenic CXCL12-Expressing Stromal Cell Subset in Murine Bone Marrow, *J Bone Miner Res* 36(6) (2021) 1145-1158. 10.1002/jbmr.4282

[68] X. Li, M.S. Ominsky, Q.T. Niu, N. Sun, B. Daugherty, D. D'Agostin, C. Kurahara, Y. Gao, J. Cao, J. Gong, F. Asuncion, M. Barrero, K. Warmington, D. Dwyer, M. Stolina, S. Morony, I. Sarosi, P.J. Kostenuik, D.L. Lacey, W.S. Simonet, H.Z. Ke, C. Paszty, Targeted deletion of the sclerostin gene in mice results in increased bone formation and bone strength, *J Bone Miner Res* 23(6) (2008) 860-9. 10.1359/jbmr.080216

[69] S. Tanaka, T. Matsumoto, Sclerostin: from bench to bedside, *J Bone Miner Metab* 39(3) (2021) 332-340. 10.1007/s00774-020-01176-0

Figure Legends

Figure 1 – miR-324-null show an increased bone mass phenotype. (a) Representative trabecular femoral µCT reconstructions are shown for male miR-324-null and WT mice aged 5-, 7- and 14-months. (b) The trabecular thickness of the femurs of miR-324-null mice are significantly increased across the time points measured, as is the trabecular SMI and the bone tissue mineral density (TMD). Trabecular thickness remains relatively constant with age regardless of genotype. Statistical significance overall across time points was assessed using two-way ANOVA and Tukey's HSD post-hoc tests were used to assess statistical significance at individual time points. (c) Three-point break test of tibia and femur from 5-month-old mice (WT n=4, miR-324-null n=5). Maximum load and displacement were determined for each bone. Statistical significance was determined using two-tailed Student's t-test. For all data *, ** and *** signify p-values ≤ 0.05, 0.01 and 0.001, respectively.

Figure 2 - miR-324-null mice display altered bone and lipid formation *in vivo*. Formalin-fixed tibial bone sections from miR-324-null and WT mice aged 7- or 14-months were stained with Goldner's Trichrome, which labels mineralised bone green, in comparison to the osteoid (non-mineralised bone), which is labelled pink. (a) Increased osteoid is observed in miR-324-null samples at both 7- and 14-months. (b) miR-324-null samples show a severe

reduction both in number of bone marrow lipid droplets and in the mean size of the lipid droplets.

Figure 3 – miR-324-null osteoblasts display increased bone formation and altered gene expression, which can be rescued by the re-introduction of physiological concentrations of miR-324. (a) Calvarial osteoblasts were isolated from miR-324-null and WT pups aged 3-5-days and cultured in osteogenic media for 7-days, after which parallel cultures were stained for alizarin red-S, assessed for alkaline phosphatase activity, or RNA extracted, and expression of key bone formation marker genes assessed. miR-324-null calvarial osteoblasts displayed increased bone formation by all of these parameters. (b) miR-324-null calvarial osteoblasts were transfected either with miCon (negative control miRNA mimic) or miR-324-5p and -3p mimics at physiological concentrations (Supplementary Figure S1) for 24 hours. (i) Osteoblasts transfected with miR-324 mimics displayed reduced bone formation, determined by alizarin red-S staining following 7-days of culture in osteogenic media. (ii) Transfection with miR-324 mimics at physiological concentrations also repressed *Col1a2* and *Runx2* expression, quantified using RT-qPCR. All groups were treated with osteogenic media for 7-days. For all RT-qPCR experiments, 18S was utilised as the housekeeping gene. For all panels, * and ** represent p-values ≤ 0.05 and 0.01 , respectively, calculated using two-tailed Student's *t*-tests. Each point represents osteoblast cultures isolated from a single mouse. (c and d) miR-324-null osteoblast transcriptome is different from that of WT osteoblasts. Osteoblasts were isolated from the femoral bones of miR-324-null and WT mice aged 20-weeks and grown to confluence before being cultured for 18 days in osteogenic media. Cells were subsequently lysed and the RNA extracted and sequenced (n=6 per genotype). (c) Volcano plot of miR-324-null versus WT osteoblasts; 3505 genes were significantly differentially expressed (adjusted p-value ≤ 0.05). (d) Samples segregated by genotype upon PCA.

Figure 4 – *Runx2* and *Cxcl12* are miR-324 osteoblast targets. (a) Of the 1596 genes significantly upregulated between miR-324-null and WT osteoblasts, 29 genes were annotated to bone- or metabolism-related Disease Ontology [24] terms. (b) In order to only test the most promising target candidates, thresholds (black lines) for the TargetScan total context score and the log₂ fold-change of < -0.25 and > 0.35 , respectively, were utilised [1, 39]. 4 genes passed these thresholds: *Cxcl12*, *Runx2*, *Top1* and *Klf7*. (c) C3H10T1/2 murine cells were transfected with 3'UTR-pmiRGLO constructs for *Runx2*, *Top1* and *Klf7* and either a negative control miRNA mimic (miCon) or a mimic of miR-324-5p or miR-324-3p. Luciferase activity was measured in cell lysates 24 hours post transfection and normalised to control Renilla activity. Values were plotted as a percentage of mean miCon luciferase activity for each construct. The *Runx2* 3'UTR resulted in a significant downregulation of luciferase activity when miR-324-5p mimic was added, an effect ablated upon mutation of 2 nt in the predicted miR-324-5p binding site. (d) Only the *Cxcl12-γ* and *Cxcl12-γ* (unique), which excludes the part of the *Cxcl12-γ* 3'UTR shared with *Cxcl12-β*, 3'UTRs resulted in a significant

downregulation of luciferase activity when miR-324 mimics were added. When 2 nt in each *Cxcl12-γ* (unique) predicted binding site of miR-324 were mutated, the ability of the miRNA to repress the luciferase gene upstream was ablated. The means of at least 4 independent experiments were used to test statistical significance, which were calculated from ≥ 3 technical replicates in each independent experiment. For luciferase assays, Student's two-tailed paired t-tests were used to assess statistical significance. *, ** and *** represent p-values ≤ 0.05 , 0.01, and 0.001, respectively.

Figure 5 – Alteration of miR-324-5p and Runx2 levels modulates the lineage commitment between adipogenesis and osteogenesis in murine C3H10T1/2 cells. C3H10T1/2 cells were transfected either with the negative control miRNA mimic (miCon), miR-324-5p mimic, the negative control miRNA hairpin inhibitor (hpCon) or miR-324-5p hairpin inhibitor (hp-miR-324-5p; at a final concentration of 50 nM). (a) After 18 days of culture in AdiOst media, cells were fixed and stained with alizarin red-S and oil red-O, as indicators of the levels of osteogenesis and adipogenesis, respectively (representative images). Stain intensity (relative to control) were quantified as described. The ratio of oil red-O to alizarin red-S intensity was termed the adipogenesis-osteogenesis (AdiOst) ratio. (b) RNA was extracted from each condition and RT-qPCR revealed that inhibition of miR-324-5p significantly increased *Runx2* expression and decreased *Pparg* expression. Overexpression of miR-324-5p significantly upregulated *Pparg*. (c) FLAG-tagged Runx2 overexpression in C3H10T1/2 cells detected by western blotting with an anti-FLAG primary antibody compared to cells transfected with a negative control plasmid (pCMV-ENTRY-neg). β-tubulin was used as a protein level normaliser. (d) Following Runx2 overexpression and 18 days of co-differentiation the AdiOst cells were stained with alizarin red-S (5X magnification) or oil red-O (40X magnification) and stain intensity and AdiOst ratio determined. Cells overexpressing *Runx2* displayed a significant increase in alizarin red-S staining intensity, a significant decrease in oil red-O staining intensity and a significant decrease in the AdiOst ratio. (e) RT-qPCR demonstrated that overexpression of *Runx2* significantly downregulated *Pparg*. Here, *, ** and *** represent p-values ≤ 0.05 , 0.01 and 0.001, respectively calculated using Student's two-tailed paired t-tests. NS, not significant. The means of 4 independent experiments were used to test statistical significance, with 3 technical replicates in each independent experiment. All RT-qPCR results were normalised using the housekeeping gene 18S.

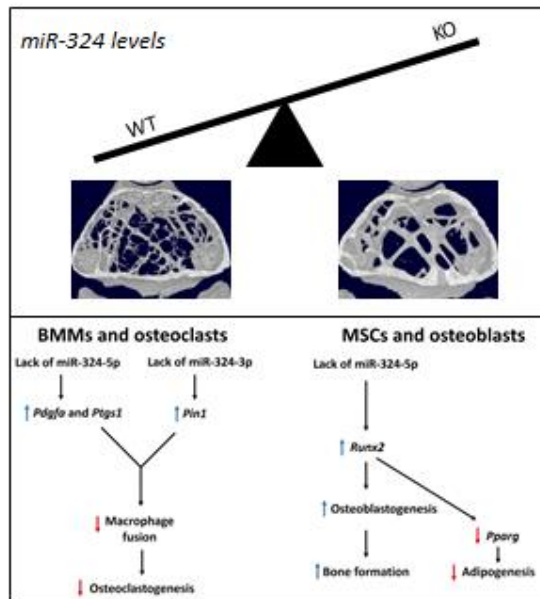
Figure 6 - Osteoclastogenesis and the haematopoietic lineage is impaired in miR-324-null mice. (a) Formalin-fixed tibial bone sections from miR-324-null and WT mice aged 7- or 14-months were stained for TRAP and analysed using TrapHisto [29]. Box indicates the higher magnification area, arrows indicate the osteoclasts. The number of osteoclasts was significantly reduced in miR-324-null samples at both ages. (b) HSCs were extracted from the bone marrow of miR-324-null and WT mice and stimulated with 100 ng/ml M-CSF for 3

days, then subsequently with 30 ng/ml M-CSF and 50 ng/ml RANK-L for a further 5 days. miR-324-null samples showed a reduction in the number of mature osteoclasts, total osteoclast area and mean number of nuclei per osteoclast. Black arrows on the representative images indicate examples of mature osteoclasts. For panels **a** and **b**, statistical significance was assessed using Student's two-tailed *t*-tests, where * and ** represent p-values ≤ 0.05 and 0.01, respectively. NS, not significant. (**c**) Volcano plots of RNA sequencing of miR-324-null and WT BMMs (M-CSF stimulated) and osteoclasts (M-CSF and RANK-L stimulated) that gave 7021 and 8865 differentially expressed genes, respectively, (adjusted p-value ≤ 0.05). Blue and orange points represent significantly upregulated and down-regulated genes, respectively. (**d**) Both BMM and osteoclast samples segregated by genotype by PCA.

Figure 7 - Important osteoclastogenesis genes are direct targets of miR-324. (**a**) Of the 3700 genes significantly upregulated between miR-324-null and WT BMMs, 42 were annotated to bone- or metabolism-related Disease Ontology terms [24]. (**b**) 9 genes passed the thresholds of TargetScan total context score and the log₂ fold-change of < -0.25 and > 0.35 , respectively; *Ccne1*, *Pdgfa*, *Klf7*, *Icam1*, *Bcl2*, *Pin1*, *Ing1*, *Ptgs1* and *App*. (**c**) C3H10T1/2 murine cells were transfected with 3'UTR-pmiRGLO constructs for each putative target gene and either a negative control mimic (miCon) or miR-324-5p or miR-324-3p. After 24 hours luciferase activity, relative to Renilla, was determined. Values are plotted as a percentage of mean miCon relative levels. The *Pin1*, *App*, *Pdgfa* and *Ptgs1* 3'UTRs were found to be targets of miR-324, with 2 nt mutation of the predicted miRNA-binding site ablating the suppressive effect of the mimic (**d**). The means of ≥ 4 independent experiments (from ≥ 3 technical replicates in each independent experiment) were used to test statistical significance. *, ** and *** represent p-values ≤ 0.05 , 0.01, and 0.001 respectively.

Figure 8 - Proposed model of the skeletal system in miR-324-null mice. In the haematopoietic lineage, *Mir324* deletion results in dysregulation of the direct target genes *Pin1* and *Pdgfa*, both of which have been purported to negatively affect osteoclastogenesis [44, 45]. In the mesenchymal lineage, dysregulation of the miR-324 target gene *Runx2* results in increased osteogenesis and reduced adipogenesis.

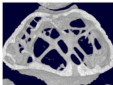
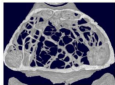
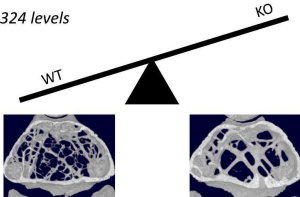
Graphical abstract



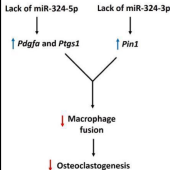
Highlights

- miR-324 has been associated with bone disease, including bone formation and in serum as a marker for fracture risk.
- Our results show that global miR-324 deletion in mice causes a high bone mass phenotype.
- Uniquely for a miRNA, null mice have both increased osteoblast and decreased osteoclast activity.
- miR-324 has a significant role in regulating mesenchymal stromal cell commitment and differentiation to adipocyte and osteoblast lineages.

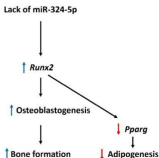
miR-324 levels



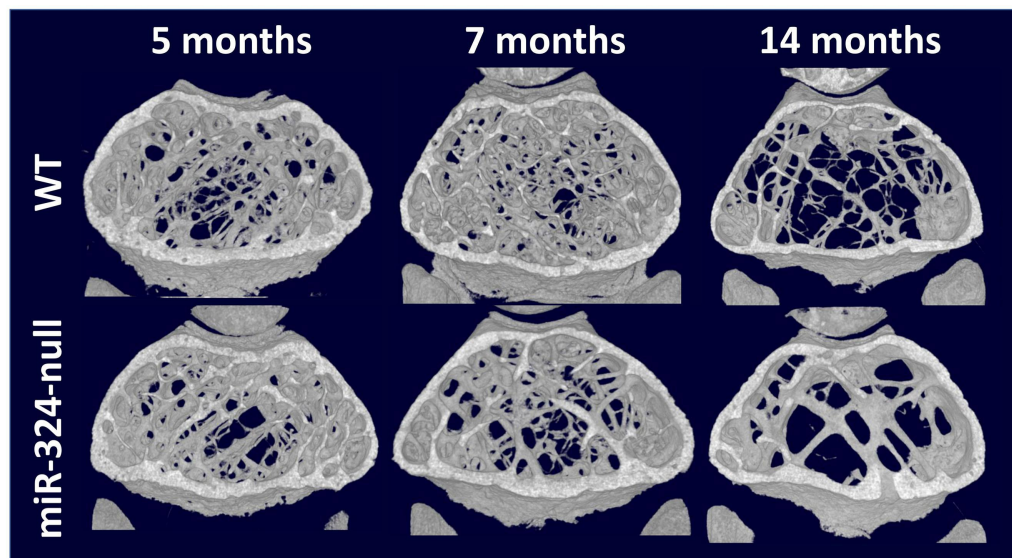
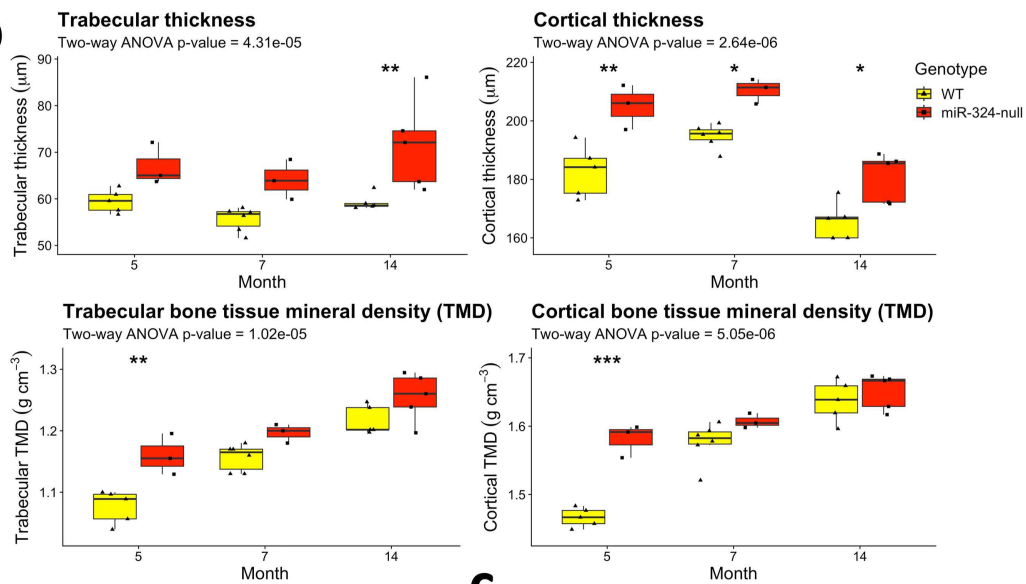
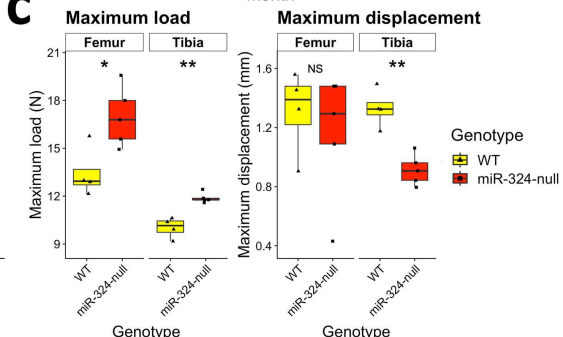
BMMs and osteoclasts



MSCs and osteoblasts



Graphics Abstract

a**b****C****Figure 1**

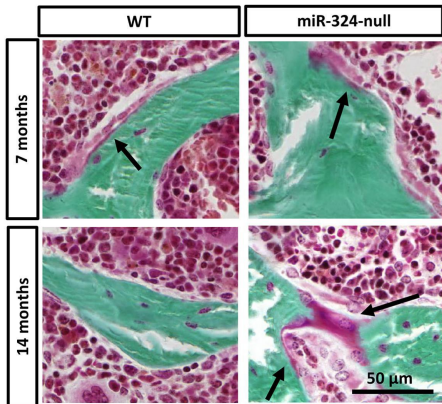
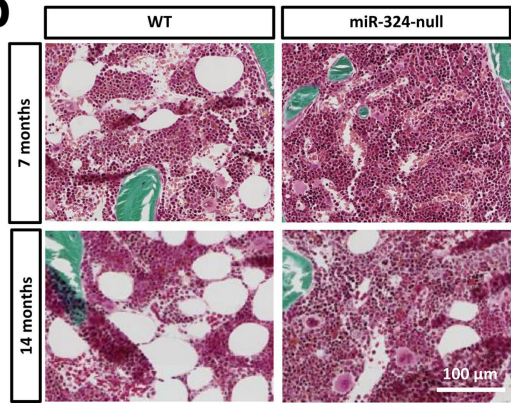
a**b**

Figure 2

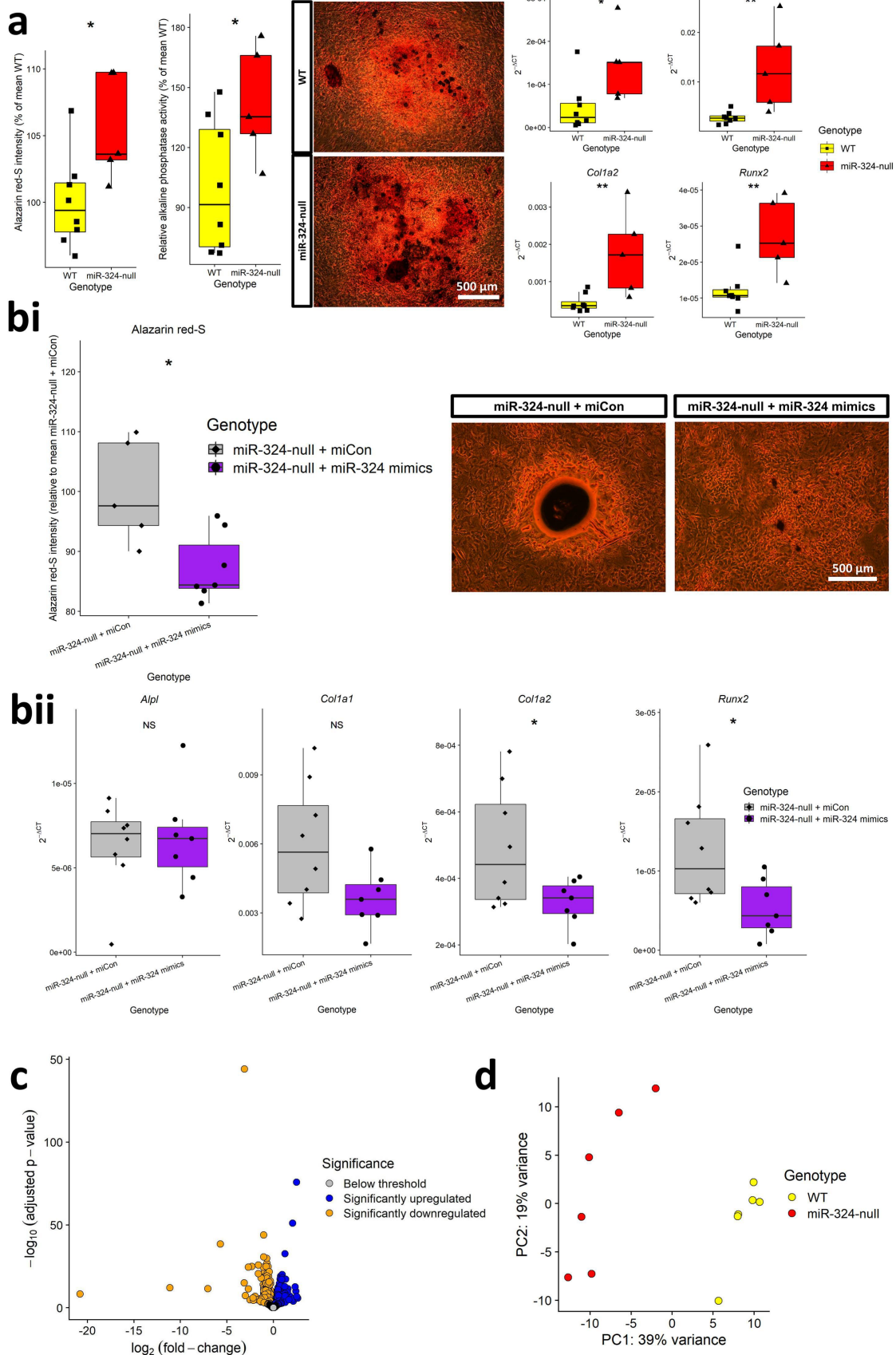


Figure 3

a

Genes significantly upregulated in miR-324-null osteoblasts

Bone disease-associated predicted miR-324 targets

Category	Count
Genes significantly upregulated in miR-324-null osteoblasts	1567
Bone disease-associated predicted miR-324 targets	334
Overlap (Genes significantly upregulated and targets)	29

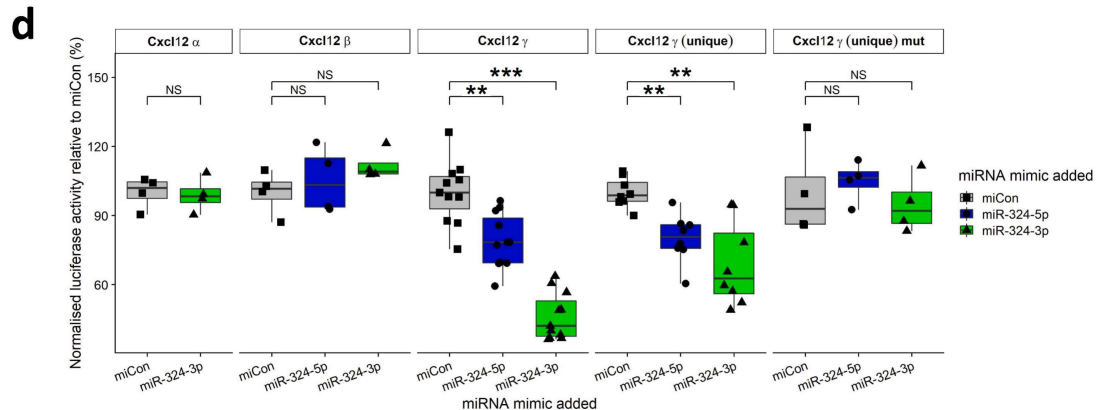
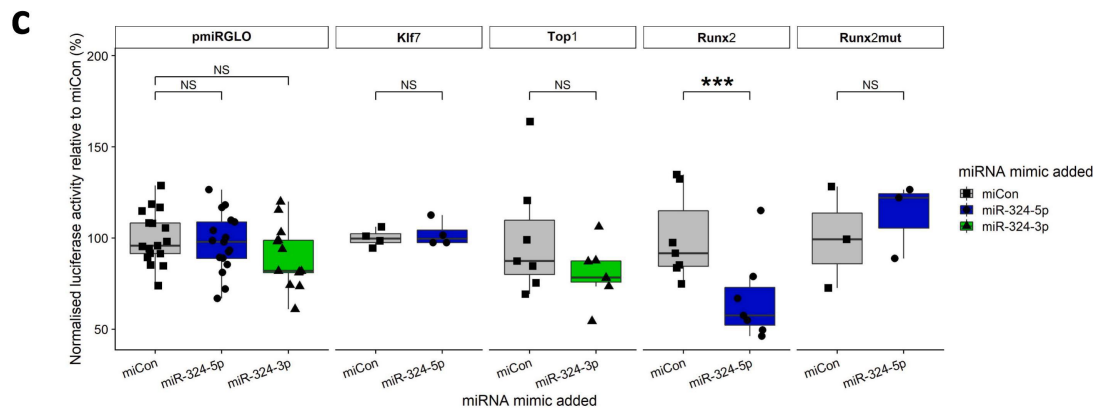
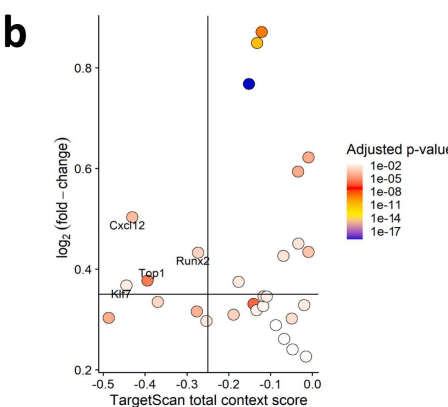
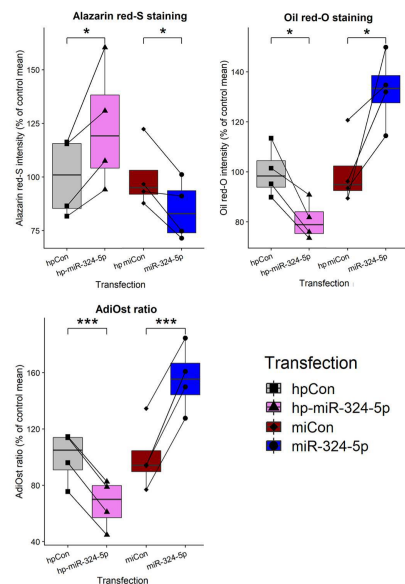
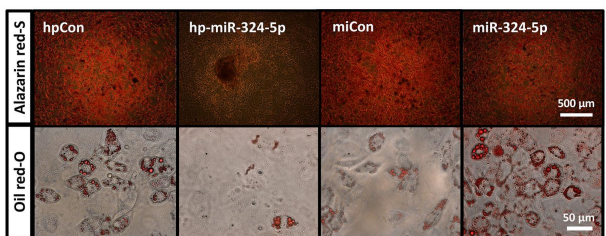
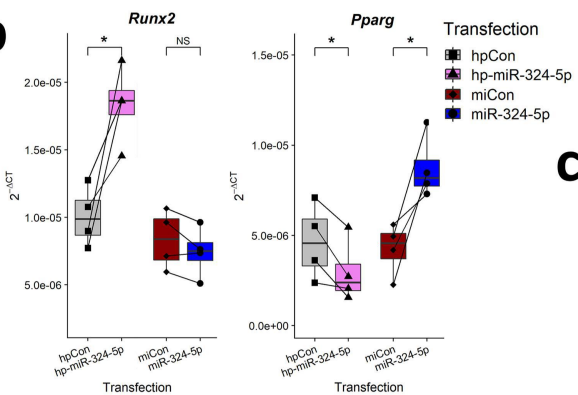
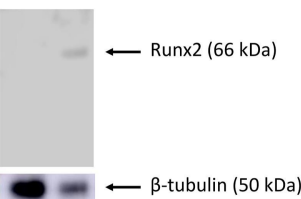
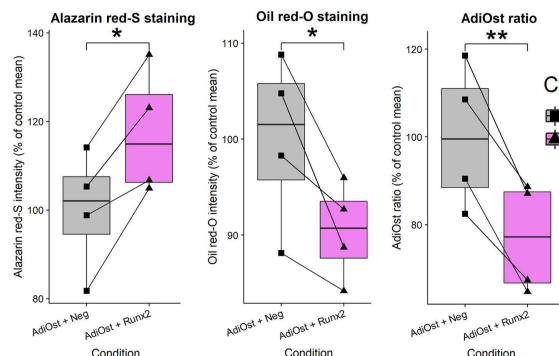
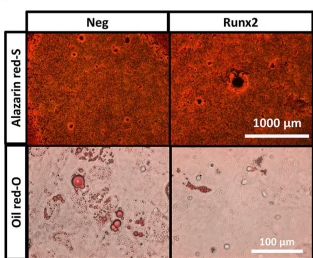
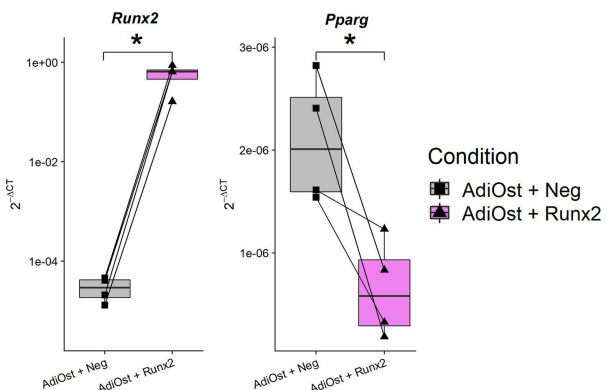
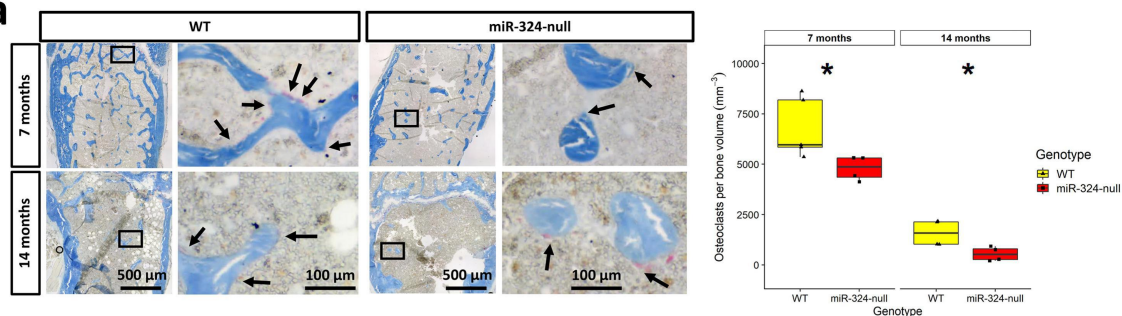
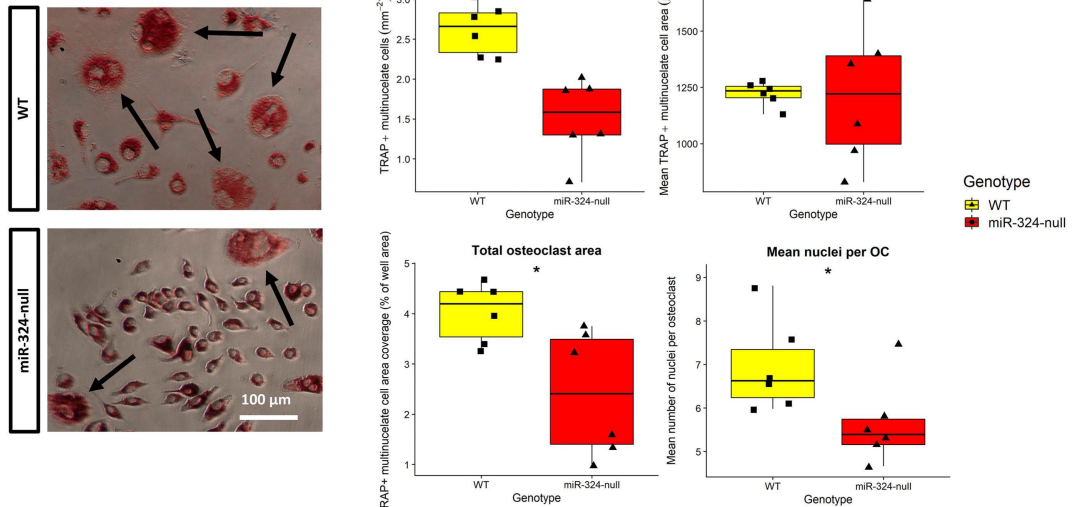
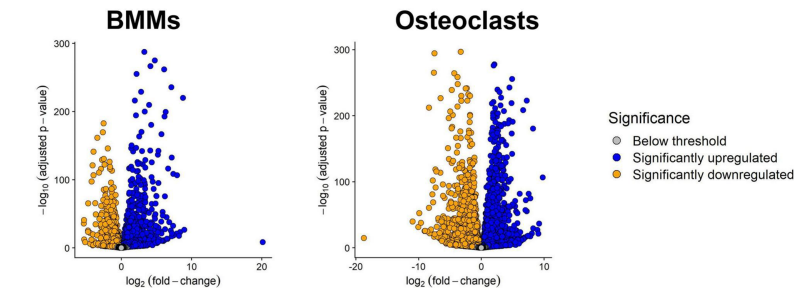
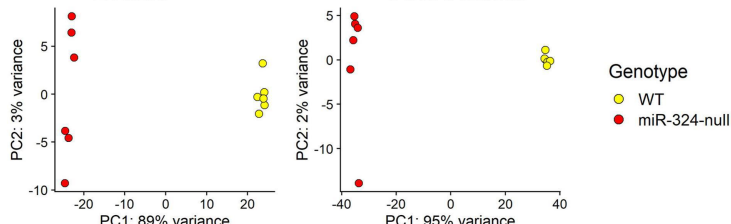
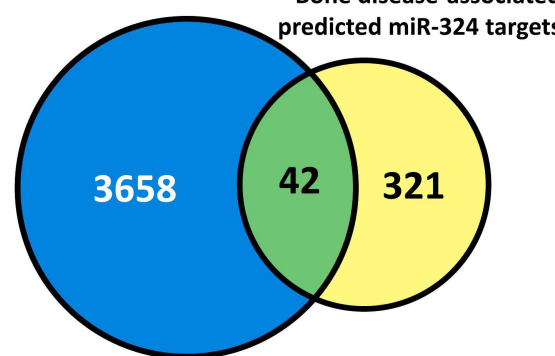


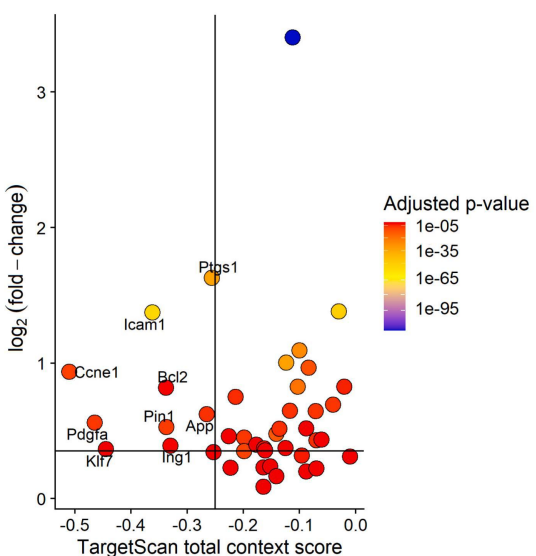
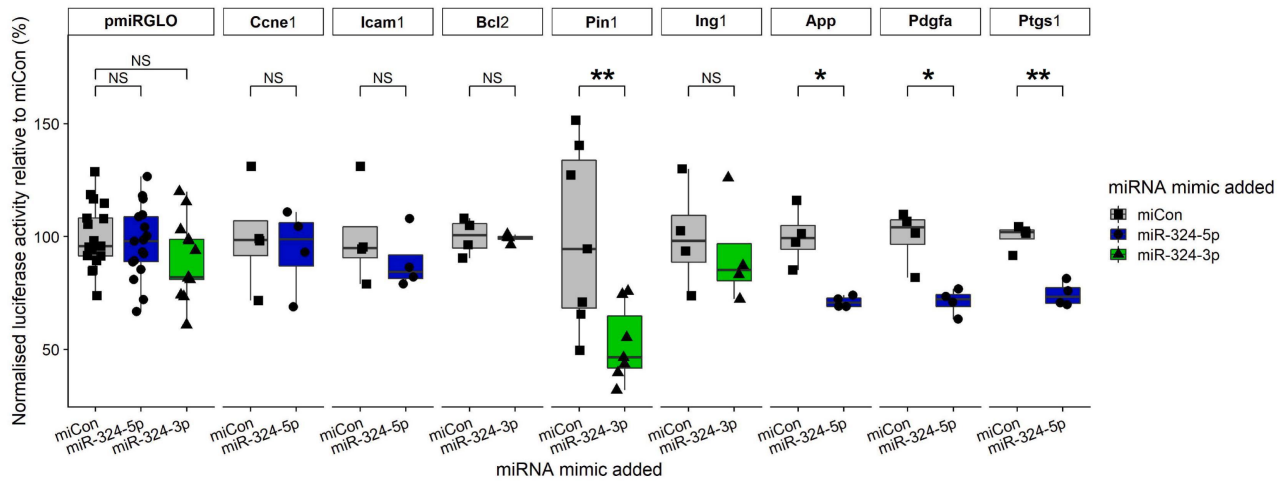
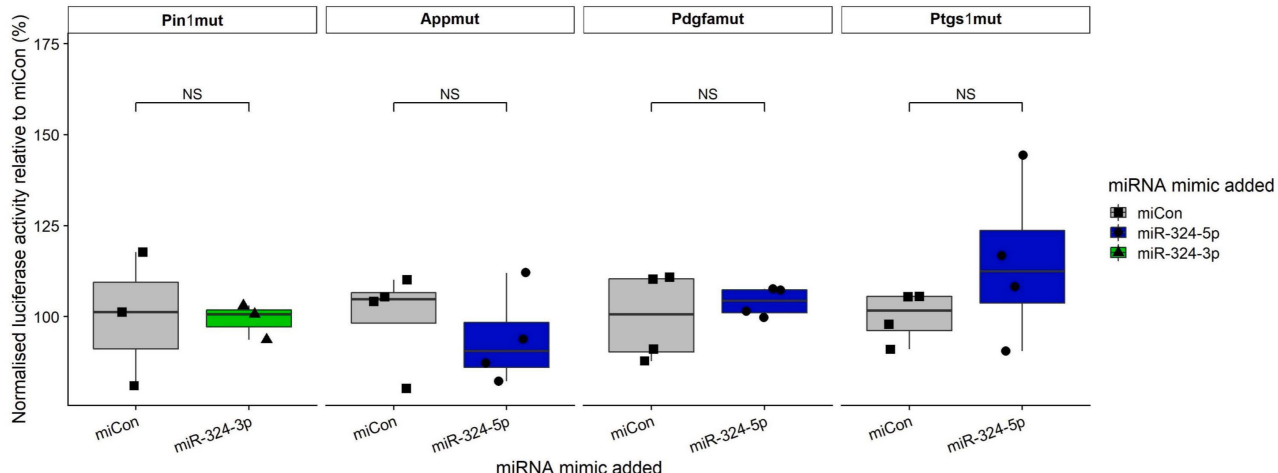
Figure 4

a**b****c****d****e****Figure 5**

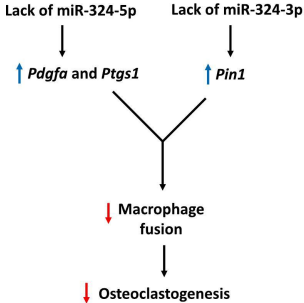
a**b****c****d****Figure 6**

a

Genes significantly upregulated in miR-324-null BMMs

b**c****d****Figure 7**

BMMs and osteoclasts



MSCs and osteoblasts

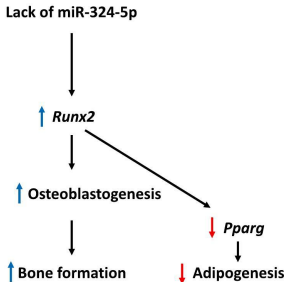


Figure 8